Sensitivity Analysis and Validation of Advanced Soil Model for OC Clays

R. O. Akporotu

Technische Universiteit Delft

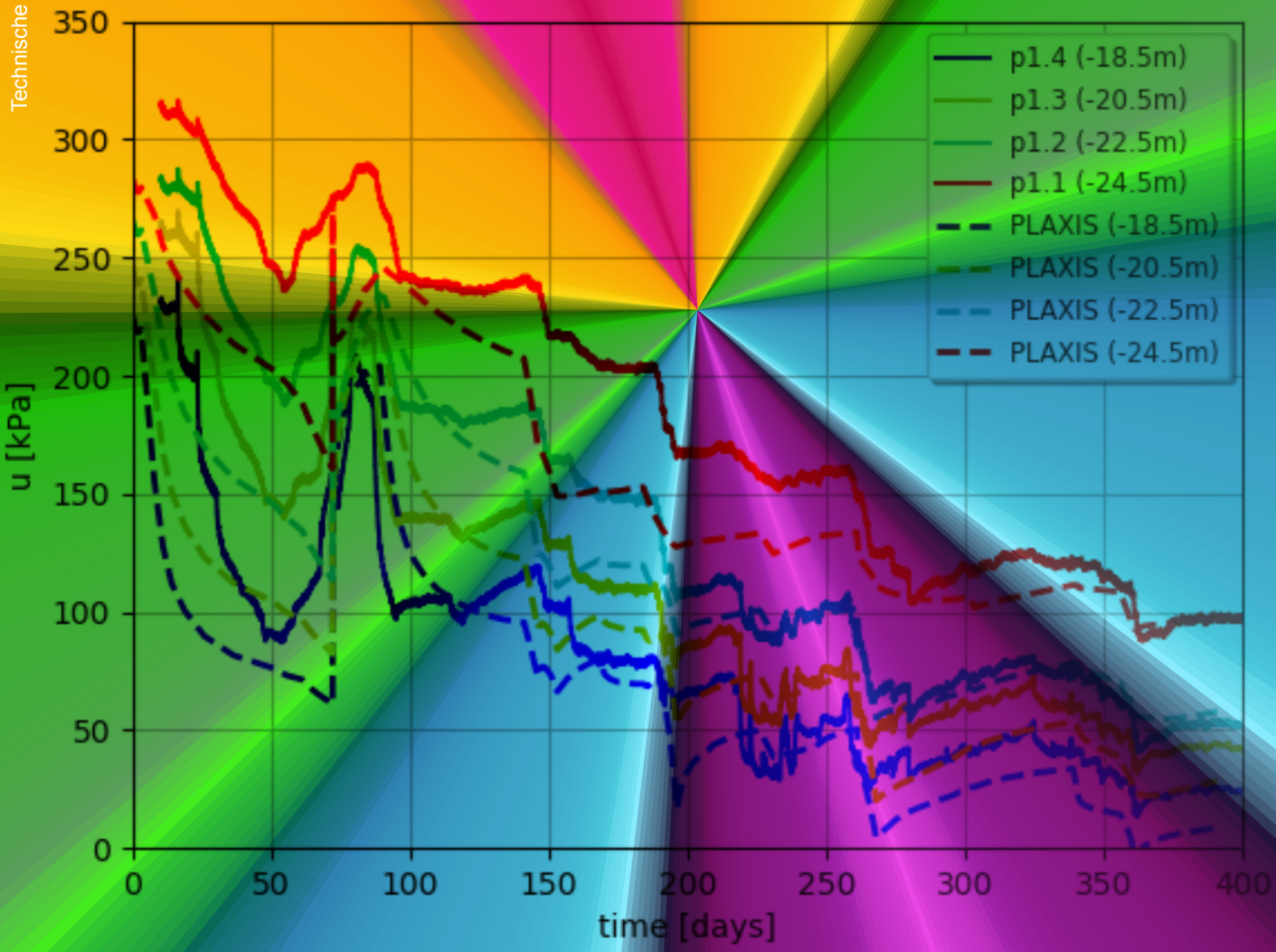

TU Delft

Sensitivity Analysis and Validation of Advanced Soil Model for OC Clays

by

Richard Onoriode Akporotu

to obtain the degree of Master of Science
at the Delft University of Technology,
to be defended publicly on Tuesday May 14th, 2019 at 13:30

Student number:	4247280	
Project duration:	September 17, 2018 – May 17, 2019	
Thesis committee:	*Prof. Michael HICKS*,	TU Delft (Committe chairman)
	Dr. Ronald BRINKGREVE,	TU Delft (University supervisor)
	Ir. Kristina REINDERS,	TU Delft
	Ir. Jan RUIGROK,	Witteveen+Bos (Company supervisor)

Faculty of Civil Engineering and Geo - Sciences (CEG)
Section Geo-Engineering (GE), TU Delft

Research is performed at Witteveen + Bos in collaboration with PLAXIS BV, a Bentley systems company

Acknowledgments

This report will be incomplete if my gratitude is not expressed to everyone that contributed to the successful completion of this thesis project. My deep gratitude goes to my daily supervisor Jan Ruigrok who's expert advice and geotechnical experience has been very valuable to this project. I would also like to acknowledge the effort of Gregor Vilhar from PLAXIS bv, who has been my mentor in soil modelling and computer programming for his encouragements and efforts in providing various versions of the PLAXIS OC Clay model used for the analysis in this project.

Special thanks to my graduation committee members, Michael Hicks for heading the graduation committee, Ronald Brinkgreve for his expert knowledge in soil behaviour which has been invaluable in this project and Kristina Reinders who have all been supportive and provided guidance through out the course of this project.

Furthermore, I would like to thank my mum for providing the means for me to study abroad in the Netherlands, my wife and daughter who has been supportive and provided a home away from my home country, my friends and family who have all been there for me during my study days.

Lastly, I will like to thank Witteveen en Bos for giving me the opportunity to perform this research, Lantis for providing the boom clay data and PLAXIS bv for the collaboration in this project which has successfully culminated into the development of PLAXIS OC Clay model and validation for boom clay.

R. O. Akporotu
Delft, May 2019

Abstract

This research has shed light on the capability of the HASP model in reproducing the dilatant behaviour of OC clays in drained and undrained conditions. The model is formulated by employing a combined hardening rule and uses the void ratio as a state variable while maintaining the simplicity of the MCC model. However, a sensitivity analysis has revealed that the model is sensitive to some input parameters which when varied slightly can largely affect the outcome of an analysis.

This has led to the formulation of the PLAXIS OC clay model while maintaining the framework of the HASP model but replacing the void ratio with volumetric strain as the state variable. Thus resulting in the use of the modified compression (λ^*) and swelling (κ^*) indexes which are used in obtaining the soil stiffness parameters used as model inputs. The PLAXIS OC clay model features the use of real soil stiffness parameters instead of soil indexes, the addition of small stain stiffness by T. Benz to improve model prediction in the small strain region and the elimination of the sensitivity issues noticed when using the HASP model.

The PLAXIS OC clay model is validated for boom clay (BC) at single stress points by simulating CU test and comparing with the available experimental data for the BC. Good agreement is found with experimental data as shown in the stress strain, pore water pressure and stress path plots obtained from the analysis.

Furthermore, the model is used to simulate boom clay in the Oosterweel trial excavation. Piezometers and extensometers are installed into the BC layer prior to the excavation to monitor the changes in porewater pressure and vertical displacement (heave) on the BC during the excavation. A comparison of the numerical and experimental data shows that good agreement is attained in porewater pressures and vertical displacement in the BC layer.

Contents

List of Figures

List of Tables

Nomenclature

Acronyms

POP	Pre-overburden pressure	kPa
2D	Two dimensional	
ASBS	Asymptotic state boundary surface	
BC	Boom Clay	
CSL	Critical state line	
CU	Consolidated Undrained	
FE	Finite Element	
HASP	Hardening State Parameter model	
HS	Hardening Soil model	
HSs	Hardening soil Model with small strain stiffness	
MCC	Modified Cam clay	
NCL	Normal consolidation line	
OC	Overconsolidated	
OCR	Overconsolidation ratio	
PLAXIS OC Clay	PLAXIS model for overconsolidated clays with small strain stiffness	
TAW	Tweede Algemene Waterpassing (Belgian Reference height system)	
URL	Unloading/reloading line	

Greek Symbols

α	Exponent in effective stress path expression in undrained condition	–
$\Delta\varepsilon_{\Gamma}$	Change in volumetric strain at a reference stress of 1 kPa on the CSL	–
$\Delta\varepsilon_{\kappa}$	Change in volumetric strain at a reference stress of 1 kPa on the URL	–
$\Delta\varepsilon_{N}$	Change in volumetric strain at a reference stress of 1 kPa on the NCL	–
η	Stress ratio (q/p')	–
Γ	Specific volume on the CSL at a mean effective stress of 1 kPa	–
$\gamma_{0.7}$	Shear strain at $0.722G_0$	–
γ_{hist}	Strain history in the loading direction used to define G_t	–
κ	Slope of swelling line	–
κ^*	Modified unloading/reloading index	–
λ	Slope of normal compression line	–

λ^*	Modified compression index	–
μ	Poisson's ratio	–
μ	Poisson's ratio	–
ω	Hardening coefficient	–
ψ'	Dilatancy angle	°
ψ_m	Mobilsed dilatancy angle	°
σ_c	Cell pressure	kPa
$\underline{\dot{\sigma}}$	Stress rate vector in hypoplastic formulation	–
$\underline{\dot{\varepsilon}}$	Strain rate vector in hypoplastic formulation	–
φ'	Effective friction angle	°
φ_m	Mobilsed friction angle	°
φ_{cs}	Mobilsed friction angle at critical state	°
ξ	Parameter in hardening rule which controls the influence of plastic shear strains on hardening parameter	–
$d\varepsilon_q^e$	Increment of elastic shear strain	–
$d\varepsilon_v^e$	Increment of elastic volumetric strain	–
$d\varepsilon_q^p$	Increment of plastic shear strain	–
$d\varepsilon_v^p$	Increment of plastic volumetric strain	–

Other Symbols

$\mathbf{L}$	Fourth order constitutive tensor in hypoplastic formulation	–
$\mathbf{N}$	Second order constitutive tensor in hypoplastic formulation	–
$\bar{p_0'}$	Mean effective stress on bounding surface	kPa
c'	Effective cohesion	kPa
d	Dilatancy	–
d_m	Dilatancy at peak stress ratio	–
E_{50}^{ref}	Reference secant stiffness	kPa
E_{ur}^{ref}	reference unloading/reloading stiffness	kPa
e_0	Initial void ratio	–
E_{50}	Secant stiffness	kPa
E_{oed}	Oedometer stiffness	kPa
E_{ur}	Unloading/reloading stiffness	kPa
f_d	Factor controlling relative density in hypoplastic formulation	–
f_s	Factor controlling barotropy in hypoplastic formulation	–
G_0	Shear modulus	MPa
G_0^{ref}	Reference shear modulus	MPa

G_t	Tangent shear modulus	MPa
G_{ur}	Unloading and relaoding shear modulus	MPa
K_{nc}^0	K_0 for normally consolidated state	–
M	Slope of critical state line	–
m	Stress dependency	–
M_f	Slope of the peak stress ratio (η) line)	–
p'	Mean effective stress on yield surface	kPa
P_f'	Mean effective stress at failure	kPa
P_κ'	Mean effective stress at the intersection of the CSL and URL in v vs ln p'plane	kPa
P_{cs}'	Mean effective stress at critical state	kPa
P_p	Preconsolidation pressure	kPa
P_{ref}	Reference stress level	kPa
q	Deviatoric stress	kPa
q_f	Deviatoric stress at failure	kPa
R_f	Failure ratio	–
v	Specific volume	–
v_ur	Poisson's ratio for unloading/reloading	–
v_0	Initial specific volume	–
v_κ	Specific volume at a mean effective stress of 1 Kpa on the URL	–
v_i	Initial specific volume	–
v_{ref}	Reference specific volume	–
N	Slope of NCL at a mean effective stress of 1 kPa	–

1

Introduction

Underground infrastructures are inevitable and necessary for urban development especially with the fast growth and development of modern cities. However the design of these infrastructures with regards to their serviceability limit state requires a thorough design based on site investigation, laboratory tests and geotechnical modelling of the soil present at the subsurface. The purpose of this research is aimed at obtaining a soil model that can provide insight regarding the geotechnical modelling of overconsolidated (OC) clays in the subsurface while utilizing the results obtained from site investigation, laboratory test and monitoring data as a means of model validation since current models fall short in unloading, e.g. tunneling situations.

1.1. Project Background and Relevance

In a bid to reduce traffic congestion, curb accidents and improve the quality of life in the Antwerp region of Belgium, it has been proposed to construct a new link (Oosterweel) to provide an alternative connection to the Antwerp ring. The Oosterweel link is approximately 10 km in length and includes a series of stacked tunnels through the Antwerp habour. A geotechnical site investigation of the area has exposed the presence of OC boom clay (BC) in the subsurface.

The time dependent behaviour of OC clays such as the ability of the soil to swell or heave usually due to a change in moisture content or the unloading of the soil (e.g. excavations, tunnels, etcetera) can cause significant damage to infrastructures resulting to economic loss due to a higher need for maintenance. The increase in volume due to the swelling of the soil can exert pressure on the tunnel lining which could resulting to cracks. For a safe design of tunnels in OC clays, it is necessary to take into account these swelling pressures and ensure that the time dependent undrained behaviour of the soil is well acknowledged.

To gain more insight about the time dependent behaviour of the BC, a trial-excavation with extensive monitoring was set up. The trial excavation is located at the Noordkasteel area of Antwerp. The motivation for choosing the location for the trial pit is based on the fact that the boom clay is found closest to the surface within the project area at a depth of approximately 23 m (TAW -17 m). The map showing the location of the trial excavation alongside the stratigraphy of the soil layer at the site are presented in the figures 1.1 and 1.2.

1.2. Problem Definition

When OC cohesive soils such as the BC are modelled with known and frequently used soil model, it is found that the strength properties and undrained behaviour are not properly taken into account. For instance, using the Hardening soil model with small strain stiffness (HSs) in undrained conditions with a zero dilatancy angle shows that the model is not capable of reproducing the dilatant behavior observed

Figure 1.1: location of trial excavation

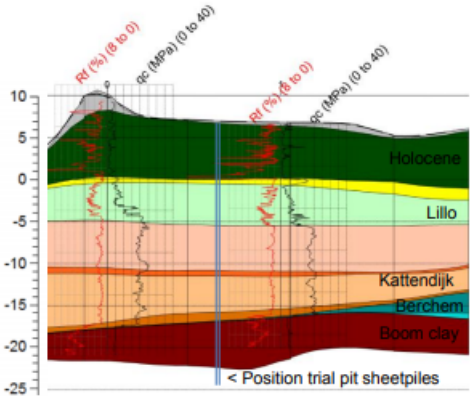

Figure 1.2: Stratigraphy of trial excavation including the measured CPT values [9]

in CU tests performed on the BC. This implies that the HSs model underestimates the strength of the BC. However including a non zero dilatancy angle in the analysis gives infinite strength and therefore is not allowed because the undrained shear strength of such cohesive soils cannot be obtained from such analysis. Furthermore, the modified Cam clay (MCC) model is also adopted to model the BC by simulating CU tests. Although, the MCC model shows some promise, the model overestimates the strength of the BC in the small strain region.

To demonstrate this, consider the undrained triaxial test performed using the soil test facility available in PLAXIS. Consolidated undrained (CU) test is performed using the HSs model (with a dilatancy angle of $0°$ and $2°$) and also with the MCC model. To aid comparison, the Initial cell pressure used is 69.4kPa which corresponds to the cell pressure used for one of the CU tests performed for the BC.The model parameters for the HSs model calibrated by A. S. Greeuw [2] for the OC BC are used for the test and is presented in table 1.1 which also contains the input parameters for the MCC model. Due to the overconsolidation of the BC, the vertical preconsolidation stress calibrated for the BC and used in the analysis is $p_p = 1050$ kPa The stress strain plot and the stress path of the tests are presented in figure 1.3 and 1.4 respectively.

Property	**Symbol**	**Value**	**Unit**
Effective cohesion	c'	20	kPa
Effective friction angle	φ'	26	°
Secant stiffness	E_{50}	10	MPa
Oedometer stiffness	E_{oed}	7.5	MPa
Unloading/reloading stiffness	E_{ur}	36	MPa
Shear modulus	G_0	145	MPa
Shear strain at $G^0 = 0.722G_o$	$\gamma_{0.7}$	2E-4	-
Reference stress level	p_{ref}	300	kPa
Stress dependency	m	0.7	-
Poisson's ratio for unloading/reloading	v_{ur}	0.3	-
K_0 value for normally consolidated state	K_0^{nc}	0.56	-
Failure ratio	R_f	0.8	-
MCC model parameters			
Property	**Symbol**	**Value**	
Poisson's ratio	v_{ur}	0.2	
Cam-Clay isotropic compression index	λ	0.077	
Cam-Clay isotropic swelling index	κ	0.026	
Slope of critical state line	M	1.11	
Initial void ratio	e_0	0.6	

Table 1.1: Model parameters

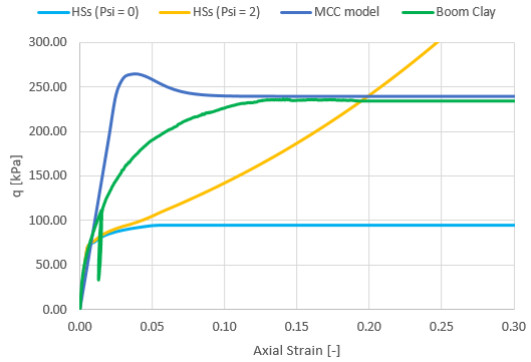

Figure 1.3: Stress-Strain plot

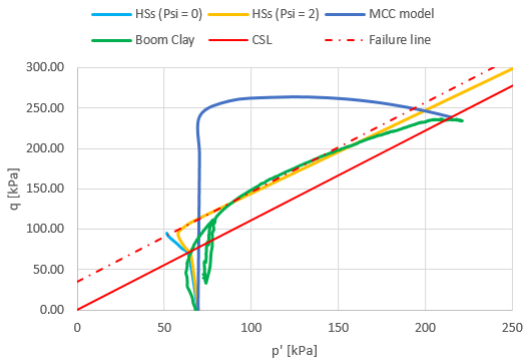

Figure 1.4: Stress path plot

The stress strain data obtained from the HSs model and MCC model are compared with the stress strain data obtained from the BC and presented in figure 1.3. The the HSs model with zero dilatancy (cyan) underestimates the strength of the BC (green) as evident in the plot. Subsequently, the HSs model with nonzero dilatancy (yellow) gives infinite strength and is unsuitable for engineering purposes. The MCC model (Blue) does not perform so badly. However between 2% and 10% strain which is the region important for engineering application, the model overestimates the strength of the BC.

A quick look at the stress path plot in figure 1.4 also shows that the HSs model with zero dialatancy (cyan) greatly underestimates the undrained shear strength of the BC. The stress path stops exactly at the failure line (dashed red) without exhibiting any dilatancy. The strength predicted by the HSs model with nonzero dilatancy (yellow) goes to infinity through the failure line without reaching the critical state (red). Although, the MCC model displays dilatant behaviour and reaches the critical state, it follows a different stress path after the first crossing of the CSL with p' remaining almost constant before failure is reached and overestimates the strength of the BC in the dilatant region as evident in figure 1.4.

The excess pore pressure built up in the sample during the test are also plotted and compared with the data obtained from the BC. As expected, the pore pressures obtained from the HSs and MCC models are not in agreement with the pore pressures recorded for the BC as seen in figure 1.5.

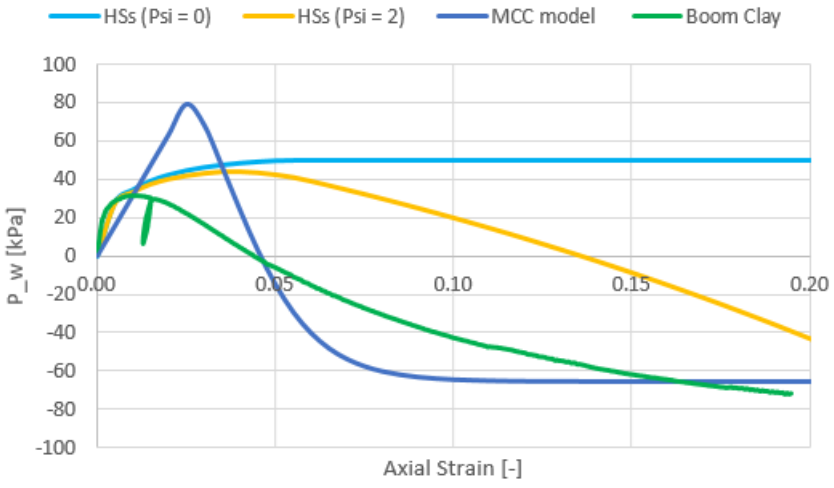

Figure 1.5: Excess porewater pressure

Having observed the deficiencies of the soil models in modelling OC cohesive soil, this research will focus on obtaining a soil model that it is capable of correctly modelling OC cohesive soils in undrained conditions while closely reproducing the dilatant behaviour observed in such soils.

1.3. Research Question

The main and sub research questions which needs to be answered to achieve the aim of this project are stated below.

1.3.1. Main Question

How can an OC cohesive soil such as the BC be modelled correctly in undrained conditions using an advanced soil model?

1.3.2. Sub Questions

1. What is the current state of the art regarding the modelling of OC soils?
2. What is a good constitutive model to model the specific (undrained) behaviour of OC clays?
3. What is the influence of the model parameters?
4. How can the advanced soil model be verified and validated?
5. What are the guidelines for determining the model parameters?

1.4. Method of Research

The methods employed in carrying out this project are enumerated below.

- Literature study on the current state on existing OC clay models.
- Model selection and implementation in python script.
- Sensitivity analysis on model's input parameter
- Model reformulation (PLAXIS OC CLay model).
- Model validation for BC based on single stress point analysis and 2D boundary value problem of the trial excavation.
- Discussion of results and conclusion.

1.5. Aim and Objectives

The aim of this research is ***to obtain a soil model capable of modelling the OC BC in undrained conditions***. Hence, the objectives of this research are as follows:

- Model selection based on the state of the art review on existing models.
- Implementation of the selected model using controlled stress paths for first evaluation on model performance.
- To obtain the model's parameters for the BC.
- To obtain reasonable agreement by simulating CU tests and comparing with experimental data for the BC.
- To produce a 2D model of the Oosterweel trial excavation that shows agreement with monitoring data.

1.6. Report Structure

This section describes the report structure in terms of chapters and their contents. Chapter 2 deals with the literature review of the current state of the art regarding the modelling of OC cohesive soils. It also contains the the selection of a suitable soil model for the analysis based on a scoring matrix. Chapter 3 contains the detailed description of the selected (HASP) model alongside the implementation in a python script. It also contains the determination of the model parameters from the available soil test.

Furthermore, a sensitivity analysis performed on the model input parameters reveals that the model is sensitive to some input parameters thus leading to the formulation of the PLAXIS OC Clay model in chapter 4. The method of determination of the model's parameters for BC is presented in chapter 4 alongside the model evaluation by performing a sensitivity analysis on the input parameter and comparing with the HASP model.

Chapter 5 contains the validation of the PLAXIS OC clay model based on single stress point analysis by simulating CU tests while the validation of the 2D boundary value problem of the trial excavation is presented in chapter 6. The conclusion to this research is presented in chapter 7.

2

State of the Art Literature Review

This chapter provides insight on the current state of the art regarding soil models available to model OC cohesive soils. The purpose of this chapter is to evaluate the available soil models based on certain criteria such as validation of the model, number of input parameters and ease of implementation. This evaluation will further result in the selection of the most suitable model for the BC. Three different soil models namely, HASP model, improved formulation of the HS model for OC clays and the Hypoplastic Cam clay model are briefly described and presented in the following sections.

2.1. Hardening State Parameter Model (HASP Model)

The HASP model was formulated by Jockovic and Vukicevic [6] to describe the mechanical behaviour of OC clays. The model was developed to overcome the deficiencies of the Modified Cam Clay model (MCC) while retaining its simplicity as having the same number of input parameters as the MCC model. The model assumes that the soil is isotropic, plastic strains develop from the beginning of loading and that hardening parameter depends on the increments of plastic volumetric and shear strains. The bounding surface is the MCC surface and the plastic strain increment vector is always perpendicular (associate flow rule) to the yield surface.

The model uses a combined hardening rule by expressing it a function of plastic volumetric and deviatoric shear strains. It follows from the axiom of critical state theory that soils move to critical state with increasing shear strains and thus should be included in the hardening rule.This combined hardening rule ensures that the yield surface continues to expand for stress ratio values $M < \eta < M_f$ and is responsible for the 'S' shaped stress path observed in undrained conditions.

2.1.1. Validation of the HASP Model

The HASP model is capable of simulating drained and undrained triaxial condition for OC cohesive soils. The validation presented in this section was performed by S. Jockovic and M. Vukicevic [12] by using published results for drained and undrained triaxial tests performed on Kaolin and Cardiff clay respectively. For brevity, only the validation regarding the undrained triaxial compression test carried out on remoulded samples of Cardiff clay is presented in this chapter of the report. The model uses five input parameters and are presented in table 2.1.

Parameter Description	Symbol	Value
Slope of virgin compression line	λ	0.14
Slope of unloading/reloading line	κ	0.050
Slope of CSL in q- p'plane	M	1.05
Reference specific volume for p'=1 kPa on CSL	Γ	3.44
Poisson's ratio	ν	0.2

Table 2.1: Input parameters for the HASP model calibrated for Cardiff clay

The stress strain plot alongside the pore pressure plot of the CU compression test performed on Cardiff clay is presented in figure 2.1. The result is presented for two OCR values and comparison is shown

with results obtained with the MCC model and as well as experimental results.

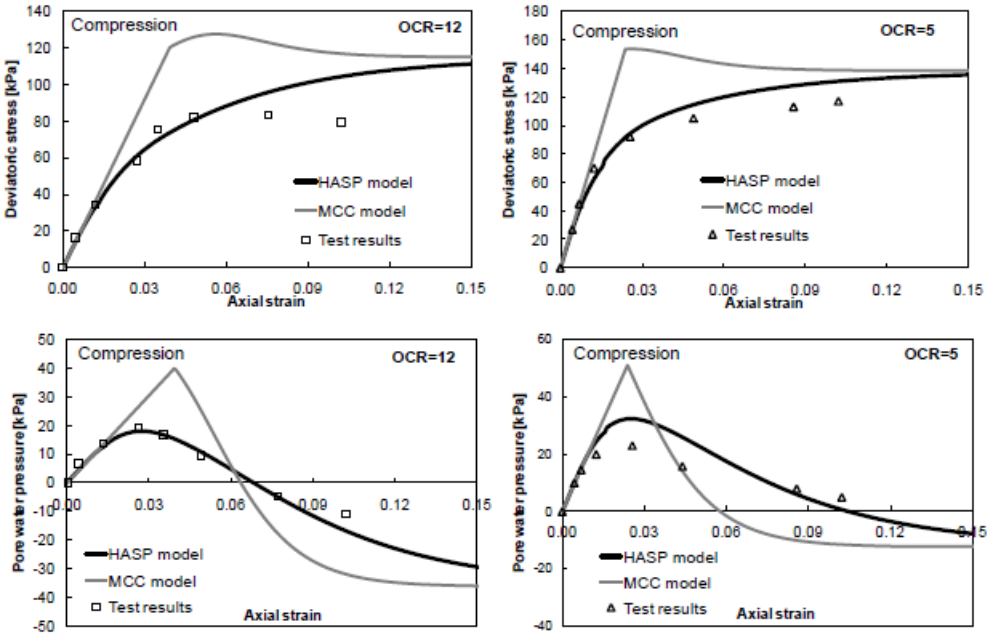

Figure 2.1: Stress - strain for Cardiff clay with different OCR values

The model shows good promise in simulating the stress strain behaviour of the soil up to 5% strain strain which is necessary for engineering applications in contrast to the MCC model which overestimates the soil strength for strains above 2%. The porewater pressures are also in good agreement with the soil data.

2.2. Improved Formulation of the HS Model by A. Truty and R. Obrzud

The second model found in literature for OC clays is an improved formulation of the HS model in the context of modelling the undrained behaviour of cohesive soils proposed by Truty and Obrzud [13] in 2015. They investigated the drawbacks experienced when using the HS model to predict the behaviour of OC clays while using a non-zero dilatancy angle.

According to their findings, the reason for this drawback can be attributed to the fact that the laws for shear and volumetric plastic mechanism are decoupled. The preconsolidation stress which is the hardening parameter of the cap yield surface depends exclusively on the accumulated volumetric plastic strain produced by the compaction mechanism. Similarly, the shear yield surface expands with increasing accumulated deviatoric plastic strain. However, due to dilatancy, the shear mechanism also produces volumetric plastic strains which is not coupled with the hardening law for the preconsolidation stress. This lack of coupling of these two plastic mechanisms leads to an unlimited undrained shear strength increase regardless of the OCR.

To solve this problem, they proposed the coupling to be done through the modification of the hardening law for the preconsolidation pressure and the correction of Rowe's dilatancy law in the dilatant domain. The coupled hardening law for the preconsolidation stress is expressed as:

$$dp_c = H\left(\frac{p_c + c\cot\varphi}{\sigma_{ref} + c\cot\varphi}\right)^m \left(d\varepsilon_v^{p,c} + d\varepsilon_v^{p,s}\right) \tag{2.1}$$

Where H is a material parameter adjusted from the assumed K_0^{NC} value and the assumed tangent oedometer modulus at a given reference stress, $d\varepsilon_v^{p,c}$ and $d\varepsilon_v^{p,s}$ are the volumetric strain increment caused by the cap and shear mechanism respectively.

The modification of Rowe's dilatancy law includes the introduction of a scalar valued function $f_c(x)$ which scales the mobilized dilatancy angle (ψ_m) with respect to the current value of OCR. This new expression for the dilatancy law is written as:

$$sin\psi_m = \frac{sin\varphi_m - sin\varphi_{cs}}{1 - sin\varphi_m sin\varphi_{cs}} f_c(x) \tag{2.2}$$

$$sin\varphi_m = \frac{\sigma_1 - \sigma_3}{\sigma_1 + \sigma_3 + 2ccot\varphi} \tag{2.3}$$

$$sin\varphi_{cs} = \frac{sin\varphi - sin\psi}{1 - sin\varphi sin\psi} \tag{2.4}$$

The function $f_c(x)$ is equal to zero for all stress paths satisfying the condition $p > p_{cs}$(effective mean stress at critical state) and nonzero (varying from 0 - 1) depending on the variable x that is defined according to:

$$x = \frac{p + ccot\varphi}{p_{cs} + ccot\varphi} \tag{2.5}$$

2.2.1. Model Verification

The verification was performed to observe the effect of the coupling, by carrying out single element tests at OCR = 1, 4, 10, 40. The initial cell pressure was set at 1000 kPa, 250 kPa, 100 kPa, and 25 kPa respectively. The model parameters of the modified HS model used are presented in table 2.2.

σ_{ref}	v_{ur}	m	E_{50}^{ref}	E_{ur}^{ref}	φ	ψ	c	R_f	H	M
100 kPa	0.2	0.5	12000 kPa	50000 kPa	24°	2°	0	0.9	12745.75 kPa	0.9215

Table 2.2: Input parameters for the modified HS model

The stress path plot simulated at different OCR values is presented in figure alongside the stress - strain plot simulated with a dilatancy angle of 2° and OCR values of 1 and 4.

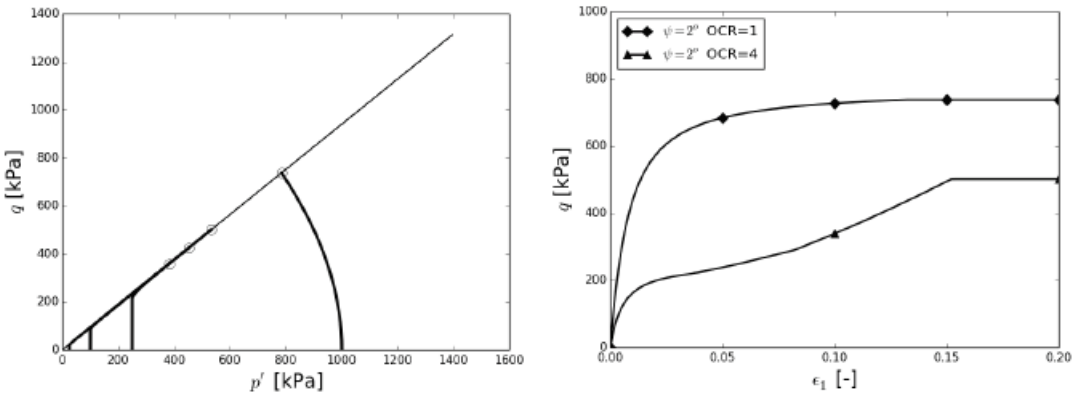

Figure 2.2: Stress path (OCR = 1, 4, 10, 40) and stress - strain obtained from the coupled model

The shortcoming of the HS model when used in undrained analysis of cohesive soils has been addressed by Truty and Obrzud [13] by the coupling of the two plastic volumetric strain mechanisms. The stress path as observed in figure 2.2 stops exactly at the critically state and no longer continues infinitely. However, the negative dilatancy which begins after crossing the CSL until failure state is reached before softening to the critical state observed in OC soils is not reproduced by the model. Also the stress strain curve for OCR 4 as seen in figure 2.2 shows too much compaction between 5% and 15% strains which is not observed in OC soils.

2.3. Hypoplastic Clay Model by David Masin

A general formulation of hypoplastic model is written as [3]:

$$\underline{\dot{\sigma}} = f_s(\mathbf{L} : \underline{\dot{\varepsilon}} + f_d \mathbf{N}||\underline{\dot{\varepsilon}}||) \tag{2.6}$$

Where $\underline{\dot{\sigma}}$ and $\underline{\dot{\varepsilon}}$ are the stress and strain-rate tensors respectively, $\mathbf{L}$ and $\mathbf{N}$ are the fourth and second order constitutive tensors, f_s is the factor controlling the influence of mean stress (barotropy factor) and f_d is the factor controlling the influence of relative density (pyknotrop factor).

The limitations of the original hypoplastic model given in equation 2.6, such as the dependency of the asymptotic state boundary surface (ASBS) on material parameters, and difficulties in further enhancing and improving the model has been identified by Gudehus and Masin [4] . For example, the constitutive tensor $\mathbf{L}$ in the original formulation does not allow for the specification of of inherent anisotropy observed in undisturbed clay samples. Any modification of this tensor $\mathbf{L}$ changes the shape of the ASBS and the possibility of further improving the model.

To solve these problems, Masin [8] proposed an explicit incorporation of asymptotic states into hypoplasticity. The shape of the ASBS is also modified to ensure good representation of experimental data and physical consistency. The model uses 4 parameters with same physical meaning as the MCC model with an extra parameter (ν/r) which needs to be determined via parametric analysis.

2.3.1. Model Predictions

To verify the effect of the proposed modification, Cu test simulations were performed by Masin for Dortmund clay, Weald clay, Koper clay, Brno clay and Kaolin clay . Only the results obtained from the simulations performed for Dortmund clay is presented in this report. The model parameters used for for the simulations are presented in table 2.3.

ϕ_c	λ^*	κ^*	N	ν/r
27.9	0.057	0.008	0.749	0.38 / 0.94

Table 2.3: Parameters used for the simulation

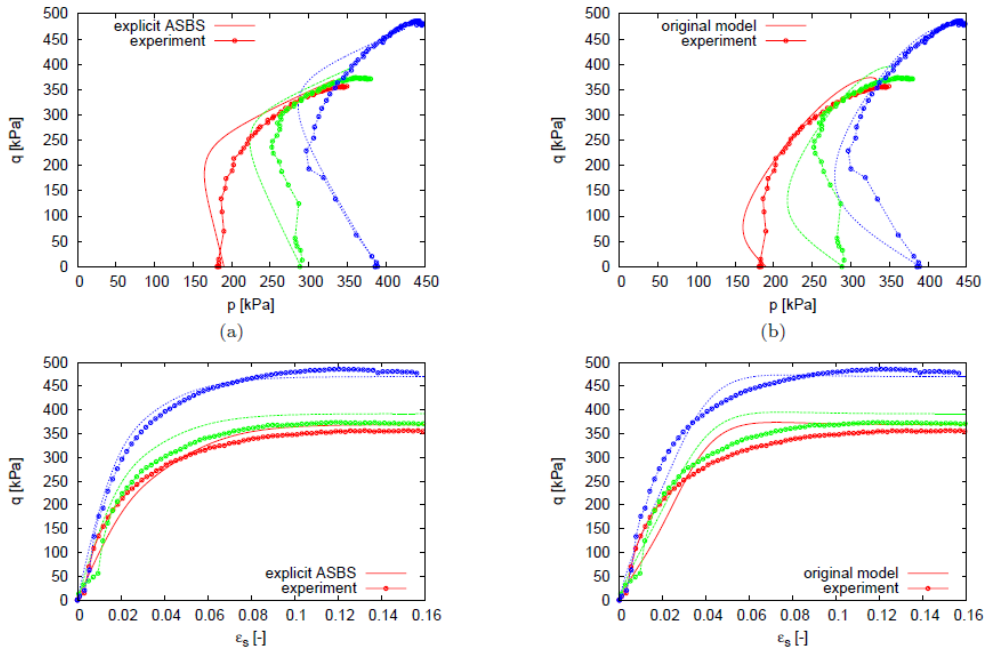

Figure 2.3: Cu tests on OC Dortmund clay and simulation by the proposed and original model [8]

The hypoplastic model described in section holds some promise in it's ability to reproduce the behaviour of OC clays. A significant improvement in model prediction is seen as the new model shows a smoother transition to failure state. However, the strain range of $0 - 5\%$ which is important in engineering application is not well reproduced. Furthermore, the presence of a material parameter which needs to be calibrated by parametric analysis and the complexity of the model implementation makes it rather difficult to choose for the analysis.

2.4. Model Selection

The three soil models presented in this chapter all show promise of being able to model OC clays. this section focuses on the selection of the most suitable model for the analysis. This selection will be made based on three selction criteria which are:

1. **Verification/Validation**
   This criteria evaluates the verification of the model for OC clays in terms of single stress point tests such as triaxial CU tests. 1 point will be given for validation that agrees with experimental result for up to 5% strain as seen in the presented stress strain and porewater pressure plots. The only test conditions considered in this evaluation is limited to CU tests because of the available CU test data for the BC. Furthermore,based on the fact that field conditions can be simulated in triaxial tests by applying a cell pressure similar to the confining stresses encountered by the soil sample insitu, this criteria can be used as an evaluation of the model's performance.

2. **Number of parameters and ease of determination**
   This criteria evaluates the model based on the number of input parameters and their ease of determination. Soil models with a lesser number of parameters which all have a physical meaning score a point.

3. **Ease of implementation**
   This evaluates the simplicity of implementing the models in a computer program for a first evaluation with the BC. This means that models that can be easily implemented without using an implicit integration schemes (which is outside the scope of this research) are favored with a point.

Selection Criteria	HASP Model	Improved HS model	Hypoplastic model
Verification / validation	Yes. Model shows good agreement up to 5% strain. (Score = 1 point)	Yes but stress strain curves for high OCR not representative (Score = 0.5 point)	Yes but model shows some disagreement with experimental results at small strains (Score = 0.5 point)
Number of parameters and ease of determination	5 parameters all obtainable from soil tests (Score = 1 point)	13 parameters with a new stiffness parameter (Score = 0.5 point)	5 parameters with one to be calibrated by a parametric analysis (Score = 0.5 point)
Ease of implementation	Moderate (Score = 1 point)	Moderately difficult (Score = 0.5 point)	Difficult (Score = 0 point)
Total score	3 points	1.5 points	1 point

Table 2.4: Model selection matrix

The model selection matrix presented in table 2.4 has shown that the most suitable model for the analysis is the HASP model based on the three chosen selection criteria. The next chapter will present the formulation of the HASP model, implementation and a quick evaluation with experimental data.

3

HASP Model

This chapter contains the formulation of the HASP model as presented by Jockovic and Vukicevic [6]. The implementation of the model in triaxial p q space by integrating along imposed stress path for undrained condition is presented alongside the model's verification with published data. Calibration and procedures for the determination of the model's parameter are also discussed. Furthermore, CU test simulations are performed with the model and compared with experimental data of the BC.

3.1. Model Formulation

The HASP model developed by S. Jockovic and M. Vukicevic [12] is formulated based on the assumptions: that the soil is isotropic, plastic strains develop from the beginning of loading and that hardening parameter depends on the increments of plastic volumetric and shear strains. The bounding surface is the MCC surface and the plastic strain increment vector is always perpendicular to the yield surface. A point A(p',q) representing a current stress state on the yield surface as shown in figure 3.1 is mathematically expressed as given in equation 3.1. The yield surface expands until peak strength is reached at stress ratio $\eta = M_f$, after which it shrinks until critical state.

$$\frac{p'}{p'_0} = \frac{M^2}{M^2 + \eta^2} \tag{3.1}$$

3.1.1. Hardening Rule for the HASP Model

The hardening rule associated to volume changes does not allow for negative dilatancy to develop before the peak strength is attained. To ensure that the yield surface continues to expand for stress ratio values $M < \eta < M_f$, a type of combined hardening rule proposed by Nova and Wood [10] is adopted where the hardening rule is expressed as function of plastic shear and volumetric strain as follows:

$$dp'_0 = \frac{v}{\lambda - \kappa} \bar{p'_0} \left(d\varepsilon_v^p + \xi d\varepsilon_q^p \right) \tag{3.2}$$

Where ξ is a parameter that connects the hardening rule with the state parameter and will be defined in the following section. The specific volume is denoted as v, λ is the slope of the virgin compression line and κ is the slope of the unloading reloading line. The combined hardening formulation allows the effective stress path to cross the critical state line (CSL) and reach the peak in drained conditions. Subsequently, this concept is the key to achieving the "s" shaped effective stress path.
Assuming the plastic shear strain increment is expressed through dilatancy as:

$$d = \frac{d\varepsilon_v^p}{d\varepsilon_q^p} \tag{3.3}$$

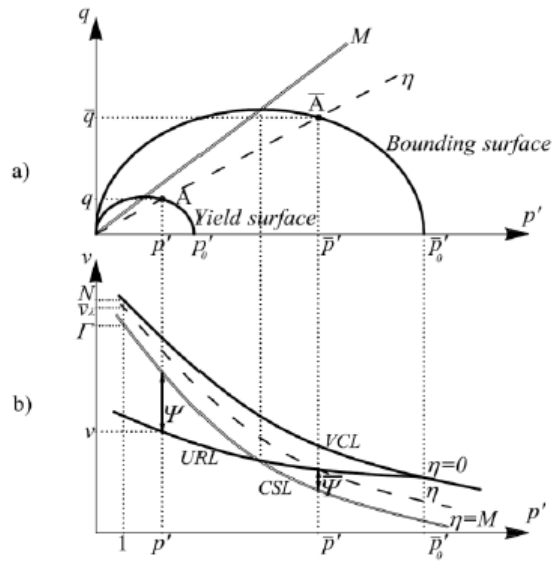

Figure 3.1: Relationship between bounding surface concept and state parameters

The current overconsolidation ratio (R) is then defined as:

$$R = \frac{\bar{p'}}{p'} = \frac{\bar{q}}{q} = \frac{\bar{p_0'}}{p_0'} \tag{3.4}$$

By substituting $\bar{p_0'}$ from equation 3.4 and $d\varepsilon_q^p$ from equation 3.3 into equation 3.2 the hardening rule can thus be re-written as:

$$dp_0' = \frac{v}{\lambda - \kappa} p_0' d\varepsilon_v^p \left(1 + \frac{\xi}{d}\right) R = \frac{v}{\lambda - \kappa} p_0' d\varepsilon_v^p \omega \tag{3.5}$$

Where ω is the hardening coefficient given as:

$$\omega = \left(1 + \frac{\xi}{d}\right) R \tag{3.6}$$

Thus, the plastic shear and volumetric strains can be expressed respectively as:

$$d\varepsilon_v^p = \frac{\lambda - \kappa}{v} \frac{1}{p'} \frac{1}{\omega} \left(\frac{M^2 - \eta^2}{M^2 + \eta^2} dp' + \frac{2\eta}{M^2 + \eta^2} dq \right) \tag{3.7}$$

$$d\varepsilon_q^p = \frac{\lambda - \kappa}{v} \frac{1}{p'} \frac{1}{\omega} \left(\frac{2\eta}{M^2 + \eta^2} dp' + \frac{4\eta^2}{(M^2 + \eta^2)(M^2 - \eta^2)} dq \right) \tag{3.8}$$

At peak strength, $dp_0' = 0$ applies and negative dilatancy becomes apparent and is denoted as d_{min}. From equation 3.6, it can be concluded that if $\omega = 0$, then $\xi = -d_{min}$. Hence it is evident that ξ is the absolute value of dilatancy at peak strength in drained conditions.

The elastic behaviour was modelled using a constant value of Poisson's ratio and the shear modulus is derived assuming isotropic elasticity from the slope of the swelling line as:

$$G = \frac{3(1 - 2\mu)}{2(1 + \mu)} \frac{vp'}{\kappa} \tag{3.9}$$

3.1.2. State Parameter Concept

As stated by the work of Li and Dafalias [7], dilatancy is not only a function of stress ratio but also depends on the state parameter Ψ. State parameter can be defined as the difference between current specific volume and the specific volume at the CSL at the same mean effective stress. From figure 3.1, the state parameter for the current stress state on the yield surface can be expressed as:

$$\Psi = v + \lambda ln p' - \Gamma \tag{3.10}$$

Where Γ is the specific volume on the CSL at a mean effective stress of 1 kPa. State parameter is negative for OC clays and positive for normally consolidated clays. However, at CSL, the state parameter is zero. Subsequently, the state parameter for conjugate point on the bounding surface is also expressed as:

$$\bar{\Psi} = (\lambda - \kappa) ln\left(\frac{2M^2}{M^2 + \eta^2}\right) \tag{3.11}$$

Furthermore, the current OCR can be expressed in terms of state parameters as:

$$R = \frac{\bar{p'}}{p'} = \frac{\bar{q}}{q} = exp\left(\frac{\bar{\Psi} - \Psi}{\lambda - \kappa}\right) \tag{3.12}$$

However, the ratio ξ/d in equation 3.6 needs to be defined. According to the authors, the parameter ξ is a constitutive constant which represents the absolute value of dilatancy at peak strength in drained condition. Parry [11] analysed drained test performed for London and Weald clay by plotting the rates of volume change at maximum deviatoric stress against the ratio p'_{cr}/p'_f (critical state mean pressure corresponding to the failure specific volume to the effective mean stress at failure) as presented in figure 3.2. By using the specific volume as the state variable, it can be shown that the ratio is a function of the state parameter in v vs lnp' plane as:

$$\Psi = \lambda ln \frac{p'_{cr}}{p'_f} \tag{3.13}$$

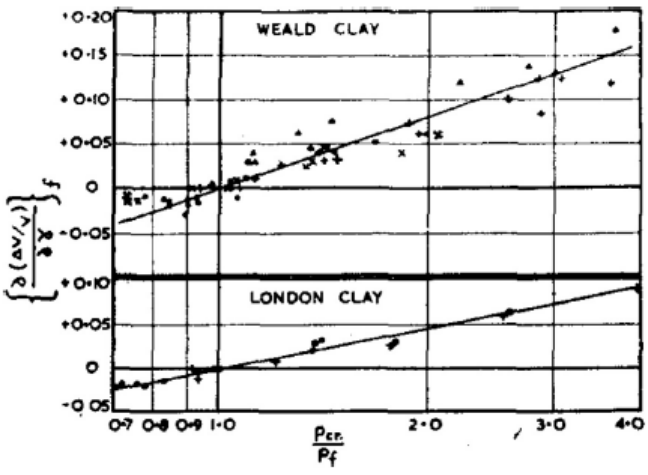

Figure 3.2: Rates of volume change at failure in drained conditions according to Parry [11]

Furthermore, Jefferies and Been [5] also stated that for OC clays and dense sands, the dilatancy is limited to a maximum value (d_{min}) for that specific soil state and that their is experimental evidence for linear relationship between d_{min} and Ψ. In addition, equation 3.12 also shows a linear relationship between the state parameter and the isotropic OCR in semi logarithmic plot. Based on the premises given above, it was assumed that the absolute value of dilatancy is on the direct dependence on the $\Psi - \bar{\Psi}$.

For stress states below the CSL, dilatancy is positive (compression) and negative (expansion) when the stress point is above the CSL while dilatancy is zero at the CSL. Therefore, dilatancy changes in a similar manner as $\bar{\Psi}$ and since dilatancy affects soil behaviour from the onset of loading till failure, the expression for the hardening coefficient is proposed as:

$$\omega = \left(1 + \frac{\bar{\Psi} - \Psi}{\bar{\Psi}}\right) R \tag{3.14}$$

It can be seen that the HASP model automatically transforms into the MCC model because for normally consolidated clays, $\Psi = \bar{\Psi}$ and the hardening coefficient $\omega = 1$

3.1.3. Characteristics of the model in undrained condition

In fully undrained conditions, there is no change in volume and hence, $d\varepsilon_v^e + d\varepsilon_v^p = 0$:

$$\frac{dp'}{p'} = -\frac{\lambda - \kappa}{\kappa} \frac{dp_0'}{p_0'} \frac{1}{\omega} \tag{3.15}$$

Re-writing the above equation by insering the the differential form of the yield surface, we gives:

$$\frac{dp'}{p'} = \frac{\lambda - \kappa}{\omega\kappa + (\lambda - \kappa)} \frac{2\eta}{M^2 + \eta^2} d\eta \tag{3.16}$$

After integration, expression for the effective stress path is then given as:

$$\frac{p_i'}{p'} = \left(\frac{M^2 + \eta^2}{M^2 + \eta_i^2}\right)^{\alpha} \tag{3.17}$$

Where p_i and η_i are initial values of the mean effective stress and stress ratio respectively. Since the hardening parameter depends on the hardening coefficient as shown in equation 3.5, it then follows that:

$$\alpha = \frac{\lambda - \kappa}{\omega\kappa + (\lambda - \kappa)} \tag{3.18}$$

The four characteristics observed in the model for undrained condition are briefly explained below and presented in figure 3.3.

1. $\eta < M, \Psi < 0, \bar{\Psi} > 0, \omega > 0, \alpha > 0, d\eta > 0$
   From the onset of loading, there is decrease in change in effective mean stress, the hardening coefficient is positive for $\eta < M$ and the stress path approaches the CSL from the right.

2. $\eta = M, \Psi < 0, \bar{\Psi} = 0, \omega \to \infty, \alpha = 0, d\eta > 0$
   At this point, the first characteristic state is reached. The conjugate state parameter and the change in mean effective stress becomes zero. The stress path will move to cross the CSL due to dilatancy.

3. $\eta > M, \Psi < 0, \bar{\Psi} < 0, \omega < 0, \alpha < 0, d\eta > 0$
   When the stress ratio crosses the CSL, it follows that $dp' > 0$. Thus the stress path approaches the CSL from the left after the maximum value of the stress ratio is reached. Subsequently, the yield surface expands while the bounding surface contracts.

4. $\eta \to M, \Psi < 0, \bar{\Psi} < 0, \omega < 0, \alpha > 0, d\eta < 0$
   As deformation increases, α increases and the stress ratio decreases until it reaches critical state, i.e. $\eta = M$ and $\Psi = \bar{\Psi} = 0$ and the maximum value of the deviatoric stress (q_{max}) is reached. Here, the yield surface equals the bounding surface.

The HASP model is implemented in a python script in undrained condition to evaluate the model's result with the test data available for the BC. The method involves calculating other quantities given a small change in the mean effective stress. Hence the mean effective stress is the governing parameter from which other quantities are derived. The computational steps for integrating along imposed stress path are given in appendix 1 while the implementation of the HASP model (undrained condition) in a python script is presented in appendix 2.

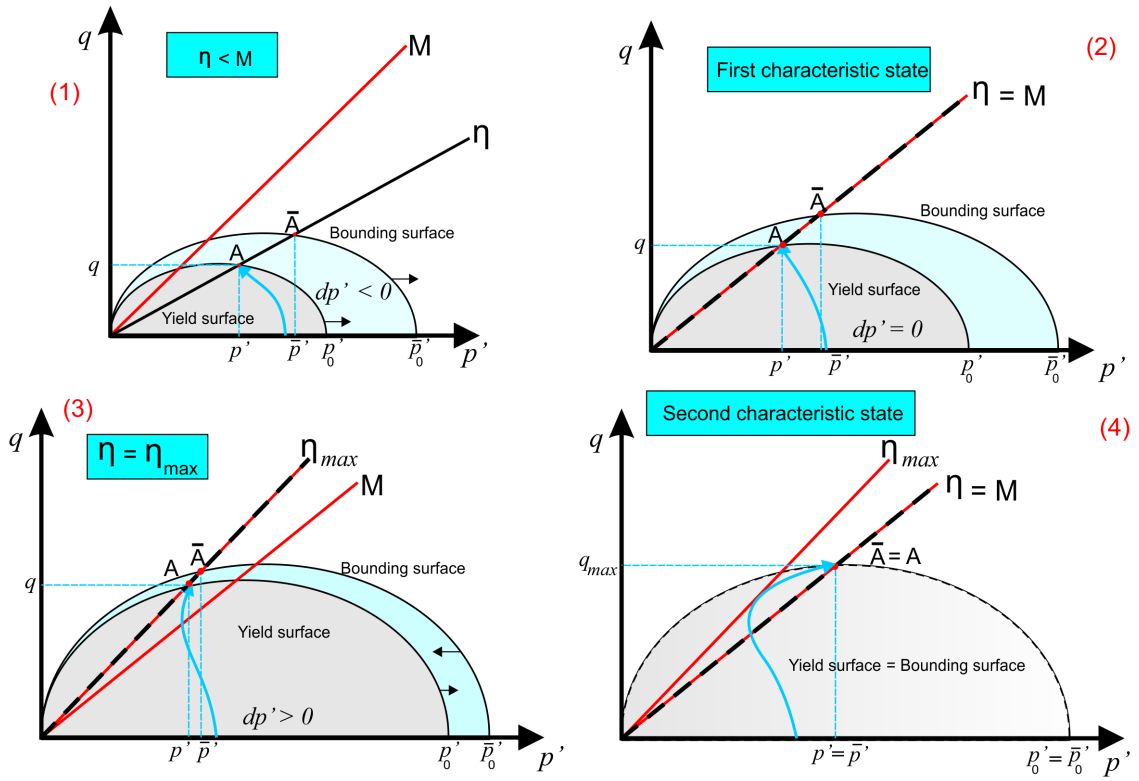

Figure 3.3: Characteristics of the HASP model in undrained condition

3.2. Model Parameters

The HASP model uses a total of 5 parameters which will be described below. The initial void ratio is also an input parameter but not a model parameter because it depends on the reference stress of the soil sample. The method of determining these parameters is also highlighted. Figure 3.4 obtained from [15] shows the visual representation of some of the model parameters.

1. **Slope of virgin compression line (λ)**
   As seen in figure 3.4, λ is the slope of the isotropic normal compression line which can also be obtained from Oedometer tests. According to Ladd and de Groot (2003), the lambda of a soil sample can be determined from an Oedometer test that is loaded up to four times the preconsolidation stress. From the available Oedometer tests, only one test(B66N5) was loaded to 1977 kPa and is used in determining the lambda for the BC. This is presented in figure 3.5.

   Taking the slope of the NCL (red line) we obtain:
   $\lambda = \frac{1.503-1.452}{6.904-7.568} = 0.077$

2. **Slope of isotropic swelling line (κ)**
   The slope of the swelling line is also obtained from the available Oedoemeter tests performed for the BC. The value of κ obtained for B55N4 BC sample is 0.022.

3. **Slope of Critical State Line (M)** The slope of the critical state line is computed as:

$$M = \frac{6sin\varphi_{crit}}{3 - sin\varphi_{crit}} = 1.113 \tag{3.19}$$

   Where: φ_{crit} is the critical state friction angle. The average value of the friction angle obtained from the soil test is $26.6°$ and the the critical state friction angle which is in principle slightly higher than the friction angle is estimated at $28°$. This value of φ_{crit} fits well with test data.

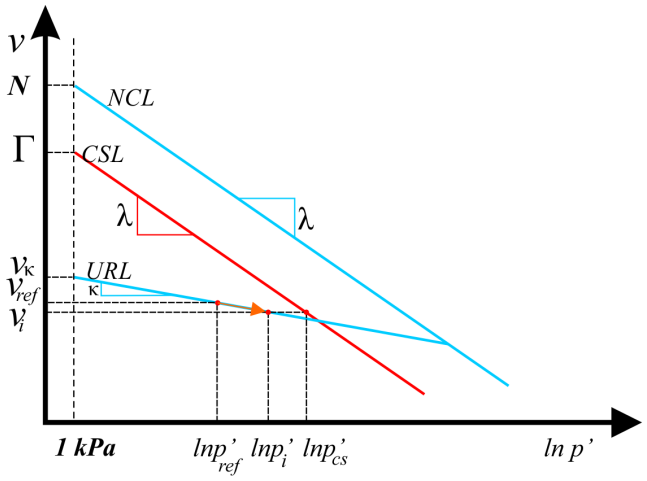

Figure 3.4: Model parameters presented in v vs lnp' space

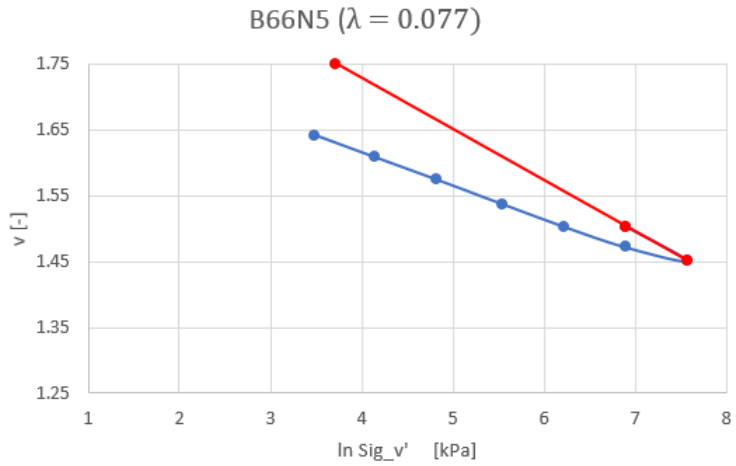

Figure 3.5: Determination of lambda as the slope of the NCL (red line)

4. **Specific volume at mean stress of 1kPa (Γ)**
   Γ can be computed from the CSL in the v vs ln P' plot. This is possible because the slope of ths CSL is also the same as lambda and thus:

$$\Gamma = v_f + \lambda ln(p'_{cs}) \tag{3.20}$$

   Where: v_f = specific volume at failure'; $p'_{cs} = p'_f$ (mean stress at failure obtained from CU test). v_f is computed based on the notion that during CU test, there is no volume change during shearing as seen in figure 3.4. Therefore, the initial volume after isotropic consolidation is the same volume observed at failure. Hence for CU test, the expression below holds.

$$v_f = v_i = v_\kappa - \kappa ln(\sigma_c) \tag{3.21}$$

   Where σ_c is the cell pressure at which the test is performed and v_κ is the specific volume at an effective mean stress of 1 kPa on the kappa line in v vs lnP' plot and is computed as:

$$v_\kappa = v^{ref} + \kappa ln(p^{ref}) \tag{3.22}$$

Where: p^{ref} and v^{ref} are the reference stress and reference specific volume respectively.

5. **Poisson's ratio (μ)**
   This is the Poisson's ratio and a value of 0.2 is typically used for this model.

6. **Initial void ratio (e_0)**
   The initial void ratio is obtained prior to commencing Oedometer test and is needed to verify the position on the v vs ln P' plot. The average value obtained for the BC is $e_0 = 0.623$. Due to the high degree of overconsolidation and overburden stress observed for the BC, the value of the reference stress at the initial void ratio is found to be $p^{ref} = 300kPa$ (in-situ stress level). Subsequently,the reference specific volume is then computed as $v^{ref} = 1 + e_0$.

The parameters for the HASP model obtained from the BC test data is summarised in table 3.1.

Parameter	λ	κ	M	Γ	μ	e_0
Value	0.077	0.022	1.113	2.043	0.2	0.6

Table 3.1: Parameters for the HASP model calibrated from BC sample B55N4

3.3. Model Verification

Prior to the commencement of the usage of the model in performing any analysis, it is important to verify that the behaviour of the model is the same as reported in literature. Verification of the model is performed using the CU test simulations performed by [6] for Cardiff clay. The model parameters used for the analysis are presented in table 3.2 and the cell presure used is $\sigma_c = 34.5$ kPa. The verification shows a perfect match between the HASP model implemented in a python script and the HASP model data digitized from literature as seen in the stress strain plot, stress path and excess pore water pressure given in figures 3.6, 3.7 and 3.8 respectively.

Parameter	**Value**
λ	0.14
κ	0.05
M	1.05
Γ	2.63
μ	0.2
e_0	0.973

Table 3.2: Parameters for the HASP model reported for Cardiff clay

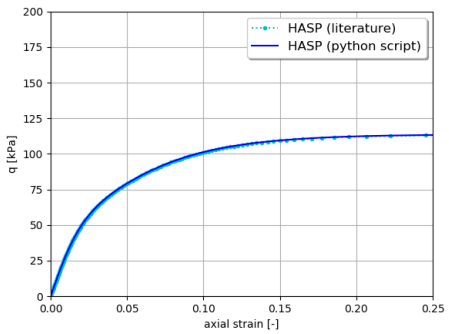

Figure 3.6: Stress-Strain plot

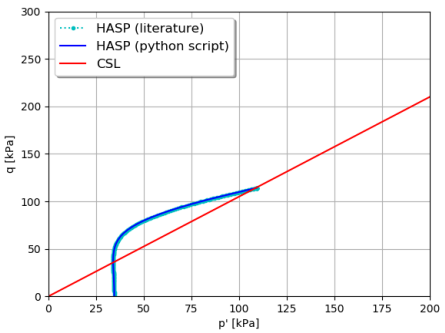

Figure 3.7: Stress path plot

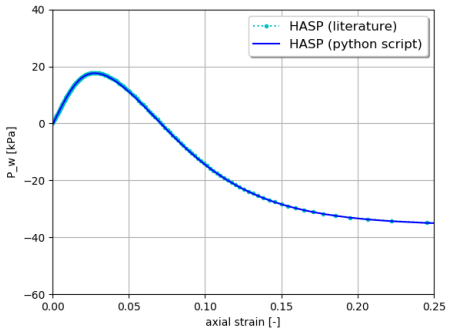

Figure 3.8: Excess porewater pressure

3.4. Simulation of CU Test

As a quick evaluation of the model's ability in describing the behaviour of the BC, a CU test is performed using the model properties of the BC presented in table 3.1. The model prediction is compared to a CU test performed for the BC sample (B55N4) at a similar cell pressure ($\sigma_c = 69kPa$). The stress strain, stress path and excess porewater pressure are presented in figures 3.9, 3.10 and 3.11 respectively.

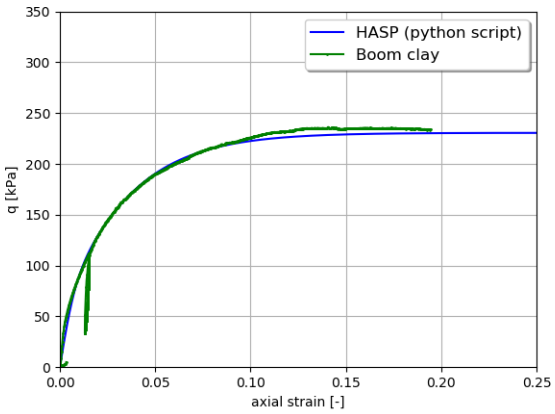

Figure 3.9: Stress-Strain plot

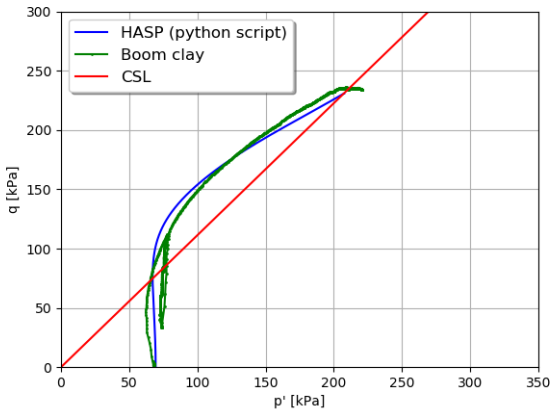

Figure 3.10: Stress path plot

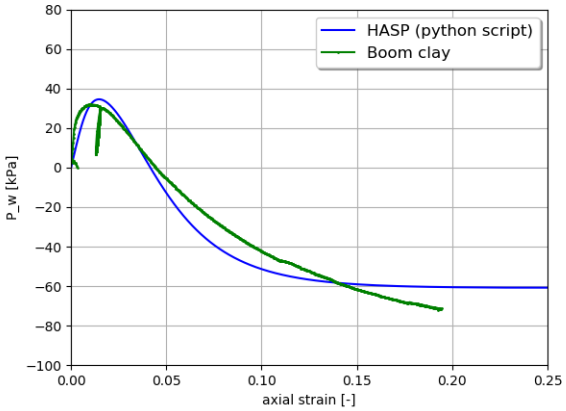

Figure 3.11: Excess porewater pressure

This section has shown that the HASP model is capable of reproducing the behaviour of the BC in undrained conditions. The stress - strain curve shows almost a perfect fit up until 10% strain. Good agreement is also observed in the stress path and the excess pore water pressure.

3.5. Sensitivity Analysis

Although the HASP model has demonstrated it's ability to simulate the behaviour of the BC, it is noticed that the model is very sensitive to some of the input parameters described below.

Sensitivity to Input Parameters (λ and Γ)
During the calibration of the BC model parameters for the HASP model, it is observed that the the HASP model is very sensitive to the input of these parameters "λ and Γ". A slight change in these parameters can significantly change the outcome of a CU test simulation.This is one of the motivations for the reformulation of the model presented in chapter 6 of this report.

To demonstrate this, a sensitivity analysis is performed by varying the Γ parameter by a 5% change. The analysis according to [6] for London clay is used to perform the CU test simulation to investigate the sensitivity of the parameters. From table 3.3 the value of Γ for London clay is given as 2.85 and a 5% change results in $5\%\Delta\Gamma = \pm 0.1425$. Hence the analysis will be performed for Γ = 2.85 $\pm 5\%\Delta\Gamma$.

The stress - strain and porewater pressure plots obtained from the the analysis are presented in figures 3.12 and 3.13 respectively. It can be seen that a 5% positive (dashed green line) or negative (solid green line) change of the parameter Γ results in a large deviation from the output of the the main data (red line). From the stress strain curves, disagreement with main data is quite visible at 1% strain.

Parameter	Value
λ	0.168
κ	0.064
M	0.80
Γ	2.85
μ	0.2
v_0	2.04

Table 3.3: Parameters for the HASP model reported for London Clay [6]

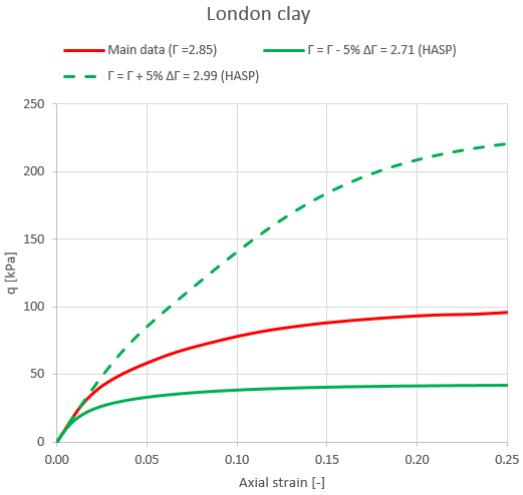

Figure 3.12: Stress-strain plot

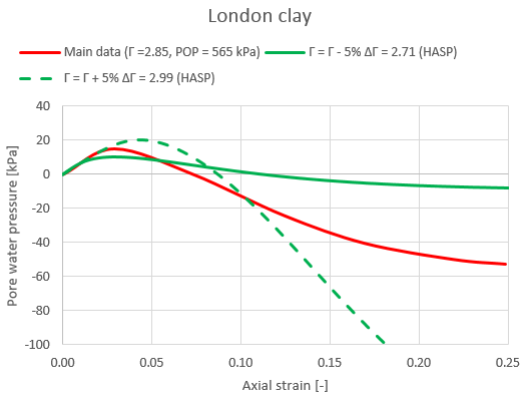

Figure 3.13: Porewater pressure

3.6. Chapter Summary

This chapter has presented the formulation of the HASP model in pq space. The evaluation of the model by simulating CU test for the BC has also yielded positive results. However, it noticed that the

model is sensitive to some input parameters which can largely affect the output of an analysis. The reformulation of the HASP model to improve the model's sensitivity to input parameters and also to enhance the behaviour of the model at small strains is presented in the next chapter as PLAXIS OC Clay model.

4

PLAXIS OC Clay Model

Based on the promise shown by the HASP model in the CU test simulation for the BC presented in previous chapter, it is proposed by R. Brinkgreve and G. Villhar [14] to improve the HASP model by reformulating the model while maintaining the original framework of the HASP model. The new model is referred to as PLAXIS OC Clay model and possess the following features:

1. Uses POP as an input parameter as opposed to Γ and v_0 used by the HASP model which are sensitive to slight changes.
2. The use of real soil stiffness parameters (E_{oed} and E_{ur}) instead of soil indexes (λ and κ) as model input parameters.
3. The addition of small strain stiffness used in PLAXIS HSs model proposed by T. Benz [1] to enhance the stiffness calculations at small strains which is essential for engineering applications.

This chapter presents the formulated PLAXIS OC clay model alongside the method of parameter determination for the model. The verification of the model is performed for Bangkok clay, London clay, Cardiff clay and Kaolin clay as presented by S. Jockovic and M, Vukicevic [6] is also given in this chapter. Lastly, a sensitivity analysis performed for the PLAXIS OC clay model input parameter and compared with the HASP model is presented at the end of this chapter.

R. Brinkgreve and G. Villhar [14] employed the stiffness calculation approach established in the HSs model to reformulate the original HASP model by replacing the void ratio with volumetric strain as the state variable thus resulting in the use of the modified compression and swelling index as visualized in figure 4.1. The relationship between the modified and classical indexes are given in equations 4.1 and 4.2. The reformulation thus excludes the initial specific volume and Γ to be used as input parameter and introduces POP as a new input parameter which will all be discussed in the subsequent sections.

$$\lambda^* = \frac{\lambda}{1 + e_0} \tag{4.1}$$

$$\kappa^* = \frac{\kappa}{1 + e_0} \tag{4.2}$$

4.1. PLAXIS OC Clay Model Parameters

PLAXIS OC Clay model uses a total of 8 parameters as shown in table 4.1. It uses the pre-overburden pressure (POP) as an extra input which defines the reference stress state of the material. These parameters will described in this section alongside their method of determination. It noteworthy to mention that unlike the HASP model, the strains at a mean stress of 1 kPa are no longer needed as input parameter for the PLAXIS OC Clay model.

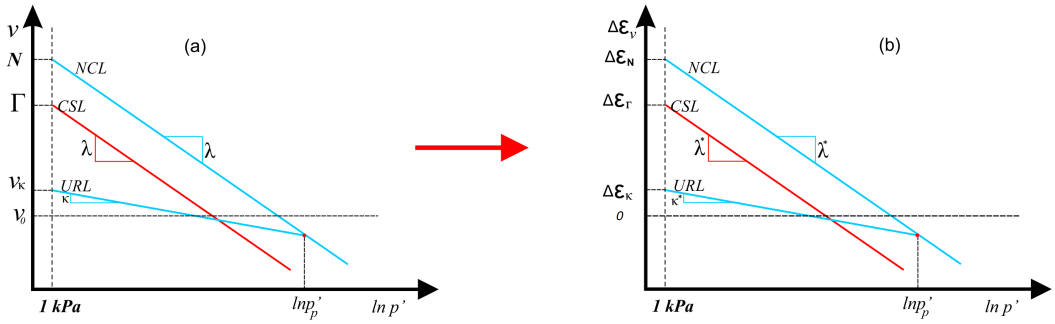

Figure 4.1: HASP model formulation (a) in v vs ln p' plane and PLAXIS OC Clay model formulation (b) in ε_v vs ln p' plane

Parameter name	Short description	Unit
E_{ur}^{ref}	Unloading/reloading stiffness	kPa
v_{ur}	Poisson's ratio for unloading-reloading	-
E_{oed}^{ref}	Oedometer stiffness	kPa
φ_{cs}	Effective friction angle at critical state	°
$\gamma_{0.7}$	shear strain at $G_s = 0.722G_0$	-
G_0^{ref}	Reference shear modulus at small strains	kPa
p^{ref}	Reference mean effective stress	kPa

Table 4.1: List of PLAXIS OC Clay model input parameters

With reference to table 4.1 and figure 4.1, it can be seen that the strains at p'= 1 kPa are no longer needed as input parameters for the PLAXIS OC clay model.

1. **Unloading and reloading stiffness (E_{ur}^{ref})**
   The elastic unloading and reloading stiffness can be calculated using the expression:

$$E_{ur}^{ref} = \frac{p^{ref} 3(1 - 2v_{ur})}{\kappa^*} \tag{4.3}$$

   Where: κ^* is the modified swelling index expressed in equation 4.2.

2. **Poisson's ratio (v_{ur})**
   This is the unloading reloading Poisson's ratio for unloading and reloading. The typical value is given as 0.2.

3. **Oedometer stiffnes (E_{oed}^{ref})**
   The reference Oedometer compression stiffnes is computed with the expression:

$$E_{oed}^{ref} = \frac{p^{ref}}{\lambda^*} \tag{4.4}$$

   Where: λ^* is defined in equation 4.1

4. **Effective friction angle at critical state (φ_{cs})**
   The effective friction angle at critical state can be calculated from the slope of the CSL with the relation:

$$\varphi_{cs} = sin^{-1}\left(\frac{3M}{6 + M}\right) \tag{4.5}$$

   Where: M is the slope of the CSL.

5. **Reference shear modulus (G_0^{ref})**
   The initial shear modulus (G_0) is estimated from a bender element test. However, this parameter

can also be estimated from CU test performed with unloading/reloading loops at small strains. The reference initial shear modulus can then be computed as:

$$G_0^{ref} = G_0 \frac{p^{ref}}{p'} \tag{4.6}$$

6. **Threshold shear strain ($\gamma_{0.7}$)**
   $\gamma_{0.7}$ corresponds to the shear strain at which, the shear modulus has reduced to 0.722 times the initial shear modulus (ε, at which:$G_s = 0.722G_0$)

7. **Reference mean effective stress (p^{ref})**
   This depends on the reference location where the sample is obtained with respect to the confining stresses. It is usually set to atmospheric pressure of 100 kPa.

8. **Pre Overburden Pressure (POP)**
   Unlike the void ratio which is an input in the original HASP model, the PLAXIS OC Clay model uses the POP as an input and can be computed with the expression:

$$POP = |p'_p - p'_i| \tag{4.7}$$

Where p'_i is the initial pressure and p_p is the preconsolidation pressure which can be obtained from oedometer test that is loaded above the p'_p of the soil using the casagrande method. However, in the absence of a representative oedometer test, p'_p can can be computed by equating the volumetric strain at the intersection of the URL and the NCL as visualized in figure 4.2, equation 4.8 holds.

$$\Delta\varepsilon_N - \lambda^* ln p'_p = \Delta\varepsilon_\kappa - \kappa^* ln p'_p \tag{4.8}$$

At the CSL:

$$\Delta\varepsilon_\kappa = \Delta\varepsilon_{cs} + \kappa^* ln p'_\kappa \tag{4.9}$$

Where $\Delta\varepsilon_{cs}$ and p'_{cs} can be obtained from CU test as: $\Delta\varepsilon_{cs} = v_i/v_0$ and $p'_\kappa = p'_{cs}$. v_i is the initial volume after isotropic compression and v_0 is the reference specific volume. p'_{cs} is the mean effective stress at failure obtained from CU test. Noting that $p'_p = 2p'_\kappa$, $\Delta\varepsilon_N$ (volumetric strain at a mean effective stress of 1 kPa) can be computed as:

$$\Delta\varepsilon_N = \Delta\varepsilon_{cs} - \kappa^* ln(2) + \lambda^* ln(2p'_\kappa) \tag{4.10}$$

Hence, p_p can be computed with equation 4.11

$$p'_p = exp\left(\frac{\Delta\varepsilon_\kappa - \Delta\varepsilon_N}{\kappa^* - \lambda^*}\right) \tag{4.11}$$

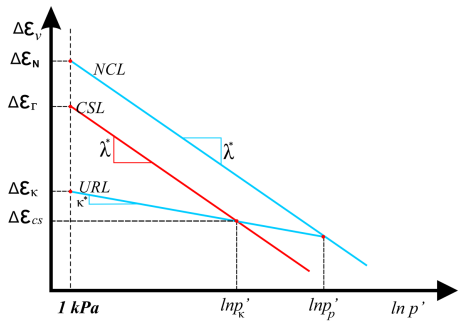

Figure 4.2: Determination of p'_p in undrained condition where $p'_\kappa = p'_{cs}$

4.2. PLAXIS OC Clay Model Verification

To check the consistency of the PLAXIS OC clay model with the original HASP model, a verification of the model is needed by comparing the outputs of both models. The verification of the model for consolidated drained(CD) test analysis is performed for Bangkok clay and Kaolin , while CU tests were performed for Cardiff clay and London clay. The results obtained from the PLAXIS OC clay model is plotted and compared with the same analysis performed using the HASP model. The HASP model data is obtained by digitizing the plots presented by S. Jockovic and M. Vukicevic [6].

The HASP model parameters used for the analysis is given in table 4.2. These were converted to the input model parameters of the PLAXIS OC Clay model using the relations provided in the preceding section of this chapter and presented in table 4.3. It is important to mention that the small strain stiffness addition of the PLAXIS OC clay model is not used in this verification of the model. Furthermore, the HASP model uses the initial specific volume (v_i) and Γ as an input specifying the test conditions while the PLAXIS OC Clay model uses POP.

	λ	κ	M	v_{ur}	Γ
Bangkok stiff clay	0.100	0.020	1.13	0.2	2.85
Cardiff clay	0.140	0.050	1.05	0.2	2.63
Kaolin clay	0.23	0.030	0.81	0.2	3.44
London clay	0.168	0.064	0.80	0.2	2.85

Table 4.2: HASP model parameters used for the analysis

	E_{ur}^{ref} [kPa]	φ_{cs}[°]	E_{oed}^{ref} [kPa]	v_{ur}	p_{ref} [kPa]	G_0^{ref}	$\gamma_{0.7}$	k_0^{nc}
Bangkok stiff clay	20506	28.5	2278	0.2	100	-	-	1
Cardiff clay	6935	26.5	1376	0.2	100	-	-	1
Kaolin clay	12540	20.9	908.7	0.2	100	-	-	1
London clay	5496	20.7	1163	0.2	100	-	-	1

Table 4.3: PLAXIS OC clay model parameters used for the analysis (without small strain for verification purposes)

From table 4.2 and 4.1, one can conclude that the original HASP model has four main parameters (λ, κ, M and Γ) whereas, the PLAXIS OC Clay model has three main parameters (E_{ur}^{ref} , phi_{cs} and E_{oed}^{ref})

4.2.1. CD test simulation for Bangkok stiff clay

Undisturbed Bangkok stiff clay obtained at depths of 17.4 - 18.0 m were used for the analysis. The cell pressures and the corresponding initial volume and POP used for the CD compression tests are presented in table 4.4. The model input parameters used for the CD test simulation for the HASP and PLAXIS OC Clay model are presented in table 4.2 and 4.3 respectively.

	Test 1	**Test 2**	**Test 3**	**Test 4**
$p'_{initial}$ [kPa]	34	103	414	552
v_i (HASP)	2.3	2.275	2.245	2.24
POP [kPa] (PLAXIS)	767.6	727.5	439.4	293.4

Table 4.4: Initial conditions for Bangkok stiff clay

The stress strain plot, stress ratio and volumetric strain vs axial strain plots obtained from the analysis is compared and plotted alongside the data obtained from the HASP model and presented in figures 4.3, 4.4 and 4.5

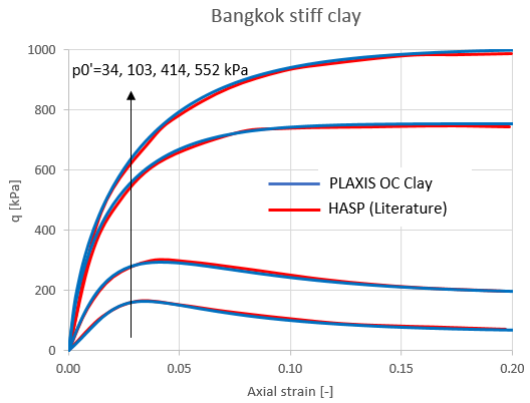

Figure 4.3: Stress-strain plot

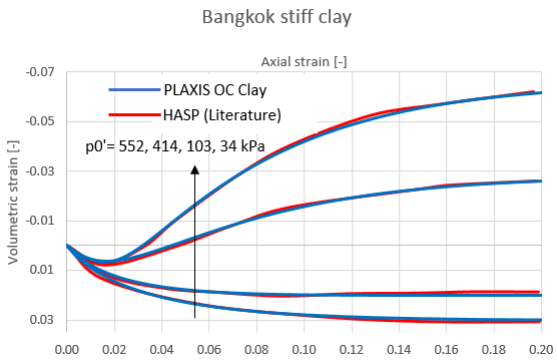

Figure 4.4: Volumetric strain

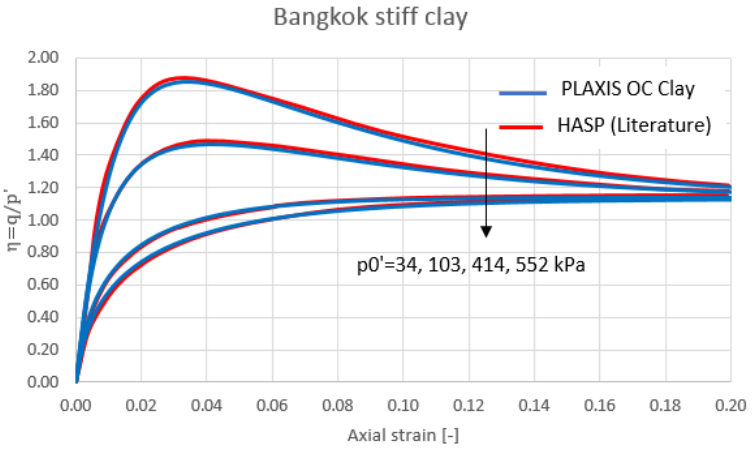

Figure 4.5: Stress ratio plot

4.2.2. CU test simulation for Cardiff clay

Remoulded samples of Cardiff Kaolin clay with a liquid limit and plasticity index of 52% and 26% respectively were used for the analysis. The initial conditions used for simulating the compression CU test are presented in table 4.5. Model input parameters used for the analysis for HASP and PLAXIS OC Clay model are presented in 4.2 and 4.3 respectively.

	Test 1	Test 2	Test 3	Test 4
OCR	12	8	5	2
$p'_{initial}$ [kPa]	34.5	48.2	73	193
v_i (HASP)	1.973	1.963	1.947	1.893
POP [kPa] (PLAXIS)	379.5	336	291.5	194

Table 4.5: Initial conditions for Cardiff clay

The stress strain plot, normalised stresspath and excess porewater pressure plots obtained from the analysis is compared and plotted alongside the data obtained from the HASP model and presented in figures 4.6, 4.7 and 4.8

4.2.3. CD test simulation for Kaolin clay

The cell pressures and the corresponding initial volume used for the CD compression tests are presented in table 4.7. The remoulded black Kaolin clay used for the analysis were isotropically consolidated to a mean effective stress of 800 kPa and subsequently unloaded to cell pressures of $p_{initial}$ = 100, 200 and 400 kPa before shearing thereby resulting to OCR values of 8, 4 and 2 respectively. The model input parameters used for the CD test simulation for the HASP and PLAXIS OC Clay model are

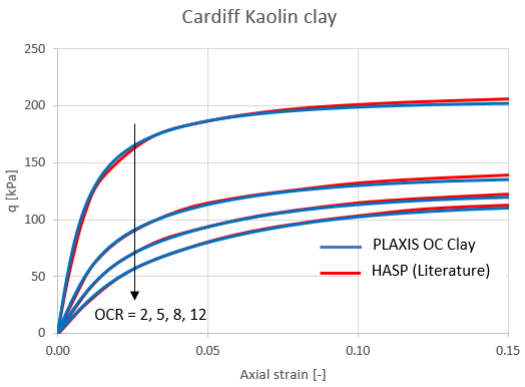

Figure 4.6: Stress-strain plot

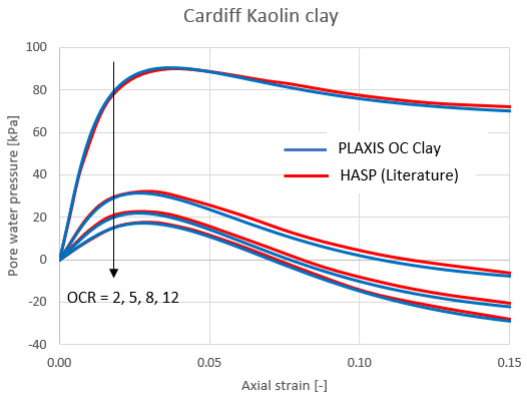

Figure 4.7: Porewater pressure

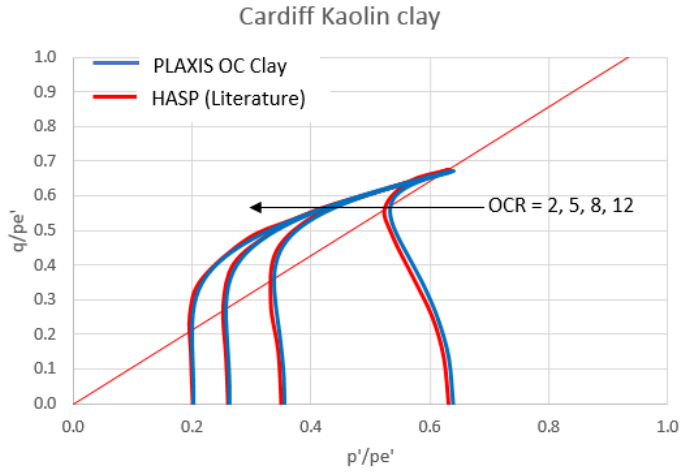

Figure 4.8: Normalised stress path plot

presented in table 4.2 and 4.3 respectively.

	Test 1	Test 2	Test 3
OCR	8	4	2
$p'_{initial}$ [kPa]	100	200	400
v_i (HASP)	2.090	2.070	2.050
POP [kPa] (PLAXIS)	756	652.7	449

Table 4.6: Initial conditions for black Kaolin clay

The stress strain plot, stress ratio and volumetric strain vs axial strain plots obtained from the analysis is compared and plotted alongside the data obtained from the HASP model and presented in figures 4.9, 4.10 and 4.11

4.2.4. CU test simulation for London clay

Remoulded samples obtained from a depth of 11 - 12 m were isotropically consolidated to before unloading to initial conditions resulting in OCR values of 20, 2.25 and 1. The initial conditions used for simulating the compression CU test are presented in table 4.7 while the model input parameters used for the analysis for HASP and PLAXIS OC Clay model are presented in 4.2 and 4.3 respectively. The stress strain plot, normalised stresspath and excess porewater pressure plots obtained from the analysis is compared and plotted alongside the data obtained from the HASP model and presented in figures 4.12, 4.13 and 4.14

The drained triaxial test performed for Bangkok stiff clay and Kaolin black clay using the HASPss model

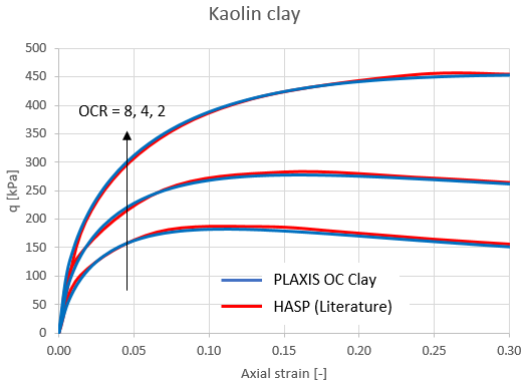

Figure 4.9: Stress-strain plot

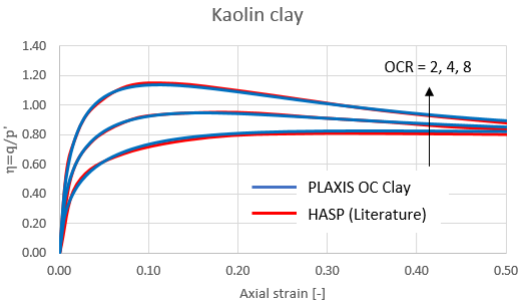

Figure 4.10: Volumetric strain

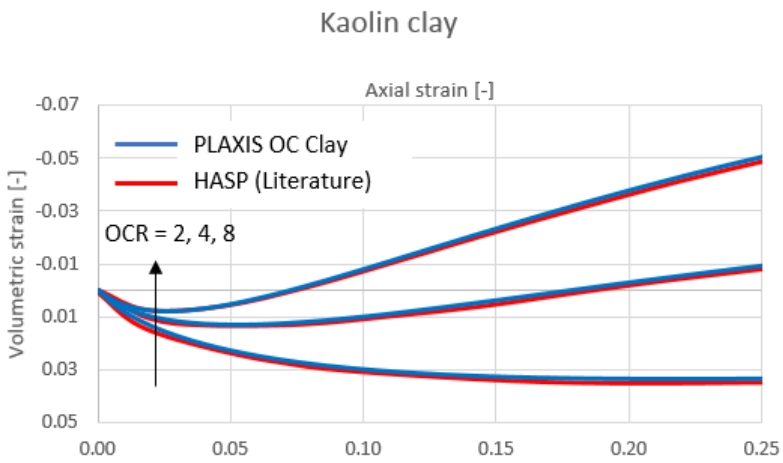

Figure 4.11: Stress ratio plot

	Test 1	Test 2	Test 3
OCR	20	2.25	1
$p'_{initial}$ [kPa]	30	200	317
v_i (HASP)	2.040	1.954	1.952
POP [kPa] (PLAXIS)	565	223.3	8

Table 4.7: Initial conditions for London clay

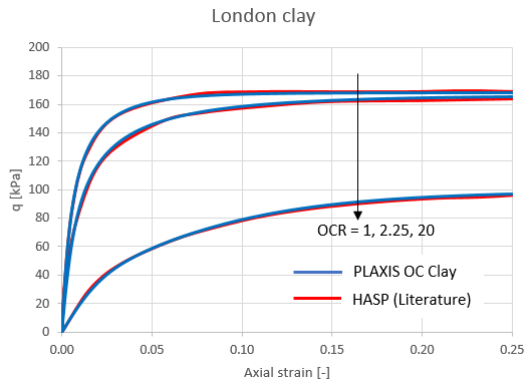

Figure 4.12: Stress-strain plot

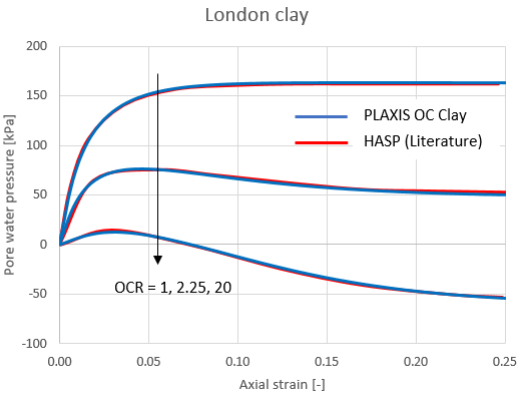

Figure 4.13: Porewater pressure

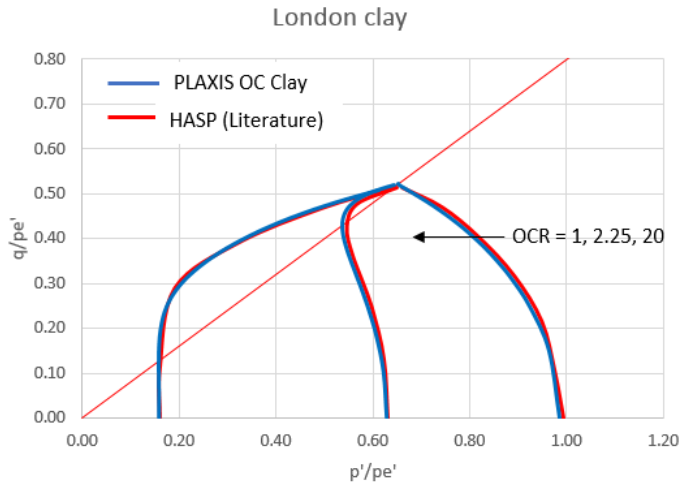

Figure 4.14: Normalised stress path plot

has shown agreement with the HASP model which helps in verifying the similarity of the model behaviour. Likewise, the undrained test performed for Cardiff clay and London clay using the HASPss model has all shown agreement with the HASP model.

This completes the verification of the PLAXIS OC Clay model to having the same behaviour as the HASP model when the small strain addition of the PLAXIS OC Clay model is not in use. The next section will focus on the evaluation of the PLAXIS OC Clay model with the HASP model to assess the improvement on the sensitivity of input parameters.

4.3. Sensitivity Analysis

To verify the improvement made by the PLAXIS OC clay with respect to the HASP model sensitivity to input parameter, CU test simulations are performed for London clay using the HASP model and presented in figures 4.15 and 4.16. Since the HASP model is sensitive to Γ and λ parameter , the corresponding input parameter in the PLAXIS OC clay is the POP parameter which is dependent on the the λ parameter. Therefore, CU test simulations are performed for London clay using the HASP model and the PLAXIS OC Clay model by varying the Γ and POP respectively by a change of 5% to observe the effect on the output in the stress - strain and porewater presure plots.

From table 4.2 the value of Γ for London clay is given as 2.85 and a 5% change results in ± 0.1425. Hence the analysis will be performed for Γ = 2.85 ± 0.1425. Using test 1 performed for London clay for the sensitivity analysis, the correspondinp POP used by the PLAXIS OC Clay model is 565 kPa. A 5% change in POP results: $POP = 565 \pm 28.25kPa$.

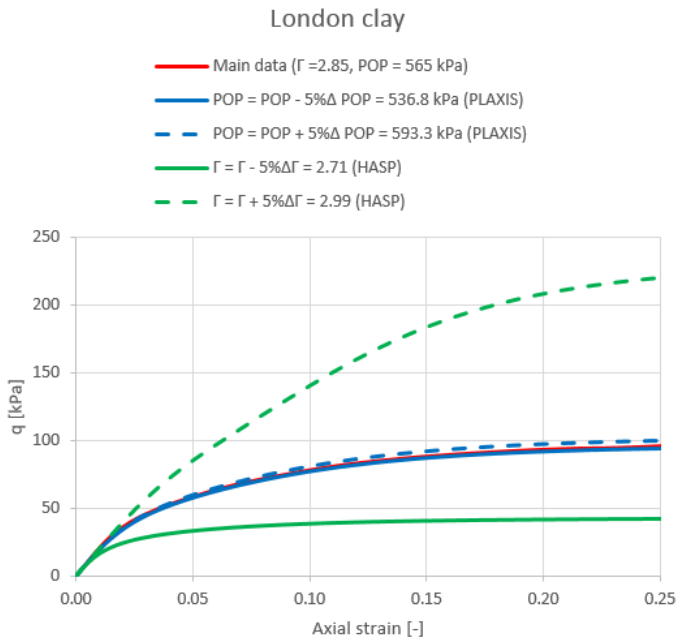

Figure 4.15: Stress-strain plot

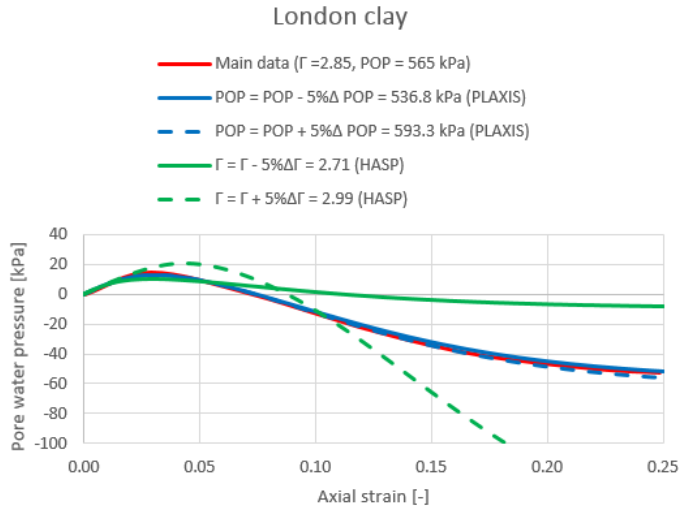

Figure 4.16: Porewater pressure plot

The stress strain and porewater pressure plots obtained from the sensitivity analysis are presented in figure 4.15 and 4.16 respectively. It is evident that from the plots that POP is a less sensitive input parameter as a 5% change results barely changes the output while a 5% change in Γ parameter for the HASP model results to large changes in output. Hence the formulation of the PLAXIS OC clay model has made it possible to eliminated the issue of sensitivity of input parameters observed in the HASP model.

5

PLAXIS OC Clay Model Validation for BC

Intact BC samples obtained between the depths of 25 - 30 m were used to perform CU compression test and Oedometer tests. Two sets CU test data are available for the validation. Test set 1 (Geo_13_060) comprises of 3 BC samples on which CU test were conducted at different cell pressures with unloading and reloading loops. Prior to the validation of the model for the BC, the influence of the small strain stiffness of the PLAXIS OC Clay model will be evaluated. Test set 2 (Geo_11_063) comprises of 7 samples on which CU test were conducted at different cell pressures without unloading and reloading loops.

5.1. Test set 1 (Geo_13_060)

The input parameters of the BC alongside the method of determination are described and listed below.

1. **Reference mean effective stress (p^{ref})**
   With respect to the overburden pressure and the depth at which the samples were obtained, the reference stress for the samples are estimated to be 300 kPa.

2. **Poisson's ratio (v_{ur})**
   This is the unloading reloading Poisson's ratio for unloading and reloading. The typical value is given as 0.2.

3. **Unloading and reloading stiffness (E_{ur}^{ref})** The average κ value calculated for the this test set is 0.026 and the initial void ratio (e_0) is found to be 0.63. Hence the modified swelling index is computed as :
   $\kappa^* = \frac{\kappa}{1+e_0} = \frac{0.026}{1+0.63} = 0.016$
   $E_{ur}^{ref} = \frac{p^{ref} 3(1-2v_{ur})}{\kappa^*} = \frac{300 \times 3(1-2(0.2))}{0.0135} = 33854kPa$

4. **Oedometer stiffnes (E_{oed}^{ref})**
   To compute the reference Oedometer stiffness, the modified compression index needs to be computed. The value of the compression index calibrated for the BC is 0.077. Hence, the modified compression index can be computed as:
   $\lambda^* = \frac{\lambda}{1+e_0} = \frac{0.077}{1+0.63} = 0.047$
   $E_{oed}^{ref} = \frac{p^{ref}}{\lambda^*} = \frac{300}{0.047} = 6350kPa$

5. **Effective friction angle at critical state (φ_{cs})**
   The effective friction angle at critical state can be calculated from the slope of the CSL with expression: $\varphi_{cs} = sin^{-1}\left(\frac{3M}{6+M}\right)$

The best fit for M for this test set is estimated at M = 1.113 and thus: $\varphi_{cs} = sin^{-1}\left(\frac{3\times1.113}{6+1.113}\right) = 28^{\circ}$

6. **Reference shear modulus (G_0^{ref})**
   The initial shear modulus (G_0) can be estimated from bender element test where one end of the plate containing the soil sample is excited and the arrival time of the signal is measured at the other end of the plate. The shear modulus is related to the shear wave velocity (v_s) and the density (ρ) by the expression:
   $G_0 = V_s^2 \rho$

   With the absence of bender element test performed for the BC, the shear modulus is estimated from CU test with unloading/reloading loops which were performed within the small strain range (γ = 1E-4 - 1E-2). Given that for CU tests, $\gamma = 3\varepsilon_1/2$, the shear modulus was computed and plotted against the shear strain for the 9 available CU tests and presented in figure 5.1. The line (blue) of best fit in figure 5.1 corresponds to the value of G_0 is 160 MPa. Stress dependency of G_0 is computed with the expression:

$$G_0 = G_0^{ref} \frac{p'}{p^{ref}} \tag{5.1}$$

   Given that the samples were obtained from a reference stress of 300 kPa and further compressed isotropically prior to shearing, G_0 presented in figure 5.1 are the reference values for the BC samples. For the simulation of CU test for test set 1, a conservative estimate of G_0^{ref} = 120 mPa fits well with test data.

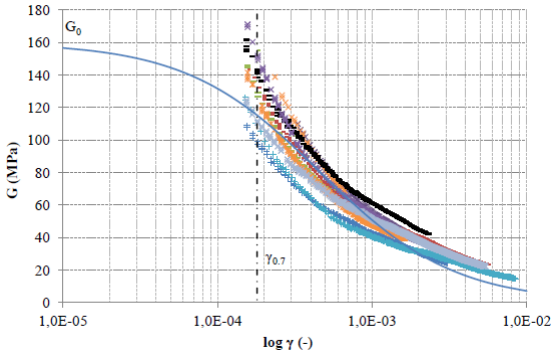

Figure 5.1: G_s computed from the unloading steps of CU tests performed for the BC [2]

7. **Threshold shear strain ($\gamma_{0.7}$)**
   $\gamma_{0.7}$ corresponds to the shear strain at which, the shear modulus (G_s) has reduced to 0.722 times the initial shear modulus (G_0). The $\gamma_{0.7}$ value calibrated by Alex [2] for the BC is between 1E-4 and 3E-4. An average value of $\gamma_{0.7}$ = 1.5E-4 is used for this analysis.

8. **Coefficient of horizontal earth pressure (k_0^{nc})**
   This is given as 1 since the sample is either isotropically compressed or unloaded during the application of cell pressure.

The model parameters calibrated for the BC were obtained from average values of CU and Oedometer tests performed for 3 different BC samples and are presented in table 5.1.

5.1.1. Small Strain Stiffness

To assess the effect of the small strain stiffness addition to the model, CU test simulations are performed with the PLAXIS OC Clay model with unloading and reloading hoops and compared with experimental data. The cell pressure and POP used for the analysis are 69.4 and 680.6 kPa respectively. The model input parameters used for the test are given in table 5.1 while the input used in simulating the test in

Parameter name	Short description	Value	Unit
E_{ur}^{ref}	Unloading/reloading stiffness	33854	kPa
ν_{ur}	Poisson's ratio for unloading-reloading	0.2	-
E_{oed}^{ref}	Oedometer stiffness	6350	kPa
φ_{cs}	Effective friction angle at critical state	28	°
$\gamma_{0.7}$	shear strain at $G_s = 0.722G_0$	1.5E-4	-
G_0^{ref}	Reference shear modulus at small strains	120	MPa
p^{ref}	Reference mean effective stress	300	kPa
K_0^{nc}	coefficient of horizontal earth pressure	1	-

Table 5.1: List of PLAXIS OC Clay model input parameters for test set 1

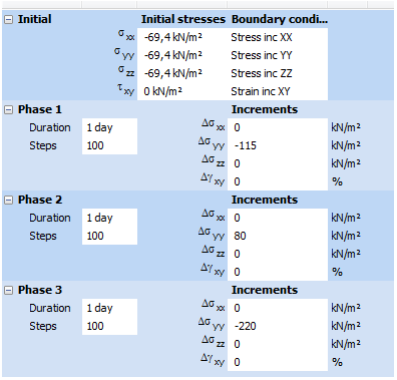

Figure 5.2: Input used in test simulation in PLAXIS

PLAXIS is presented in figure 5.2.

The stress - strain curve obtained from the analysis (figure 5.3 and 5.4) shows that the PLAXIS OC Clay model is capable of simulating unloading/reloading loops at small strain. A close inspection of the stress strain curve reveals that the model is not able to fully recover the reloading stiffness which may be due to the absence of Masin's rule attributed to the elasoplastic formulation of the model which implies that plastic strains develop from the onset of loading.

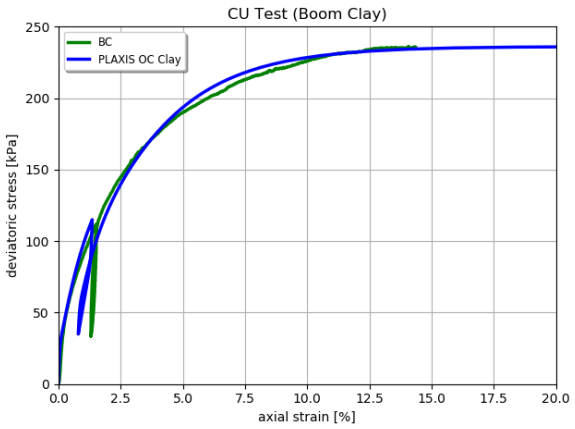

Figure 5.3: Stress-strain plot

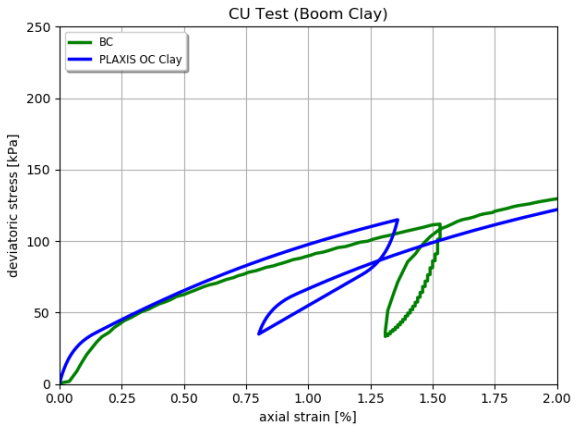

Figure 5.4: zoomed in view of the stress strain plot

The figures 5.5 and 5.6 shows the comparison of the PLAXIS OC Clay model with the HASP model. The effect of the small strain addition is evaluated by simulating CU test for BC sample B55N4 using the PLAXIS OC Clay model and the HASP model. The PLAXIS OC Clay model gives a better match with experimental data at small strains while the HASP model shows some deviation and is unable to perform unloadin/reloading loops. However, it seems like the unloading - reloading behaviour of the PLAXIS OC Clay model is not very realistic. The next section will focus on validating the BC on the

basis of available experimental data.

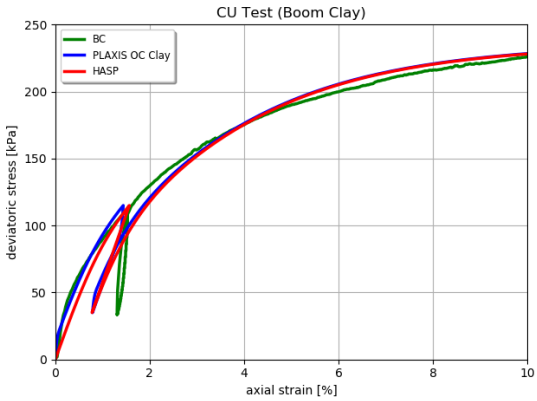

Figure 5.5: Stress-strain plot

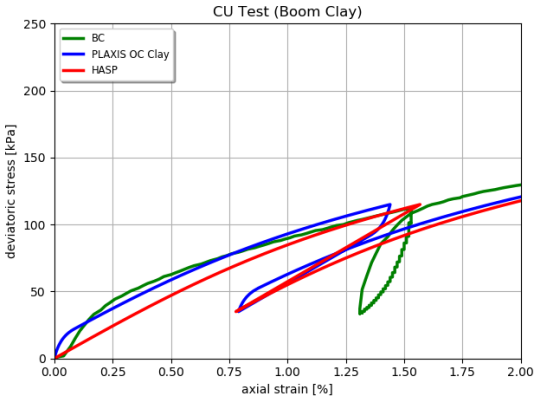

Figure 5.6: zoomed in view of the stress strain plot comparing HASP and PLAXIS OC Clay model

5.1.2. BC Sample B55N4

The B55N4 sample is obtained at depth of 27 - 27.5 m. Initial test conditions for the simulation of CU tests are presented in table 5.2

	Test 1	Test 2
p_i' [kPa]	69.4	136.3
POP [kPa]	659	592

Table 5.2: Initial conditions for BC sample B55N4

For clarity, the method for computing the POP for is given here.

Given that: $POP = |p_p' - p_i'|$, $p_p' = exp\left(\frac{\varepsilon_\kappa - \varepsilon_N}{\kappa^* - \lambda^*}\right)$.

At critical state, $p_\kappa' = p_{cs}' = p_f' = 208kPa$ (Obtained from CU test)

$\varepsilon_\kappa = \varepsilon_{cs} + \kappa^* ln p_\kappa = 1.0909$. Given that the reference specific initial volume $v_0 = 1.630$ and the initial volume after isotropic compression $v_i = 1.6681$, $\varepsilon_{cs} = \frac{v_i}{v_0} = 1.023$

Hence $\varepsilon_N = \varepsilon_{cs} - \kappa^* ln(2) + \lambda^* ln(2p_\kappa') = 1.2972$

$p_p' = exp\left(\frac{1.0909 - 1.2972}{0.016 - 0.047}\right) = 728kPa$

Therefore for test set 1, the POP input used for the test are computed using the expression: $POP = |p_p' - p_i'| = |728 - p_i'|$. Where P_i is the initial cell pressure.

The stress strain, stress path and porewater pressures obtained for the BC sample are presented in figures 5.7, 5.8 and 5.9

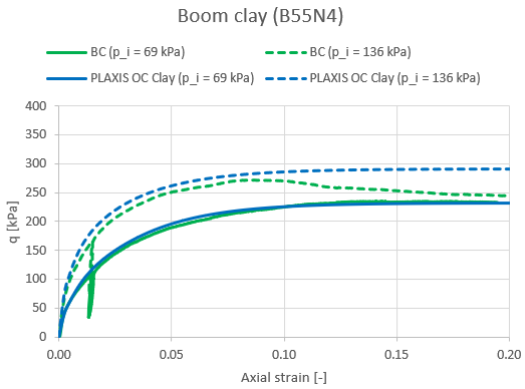

Figure 5.7: Stress-strain plot

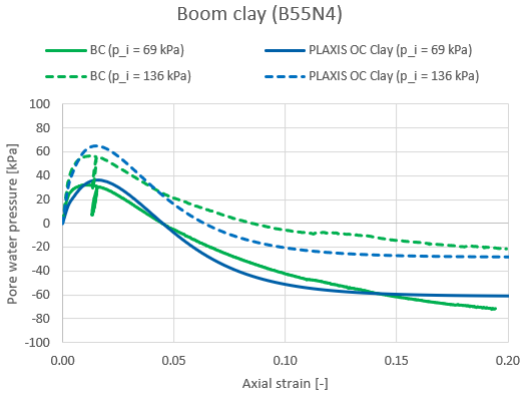

Figure 5.8: Porewater pressure

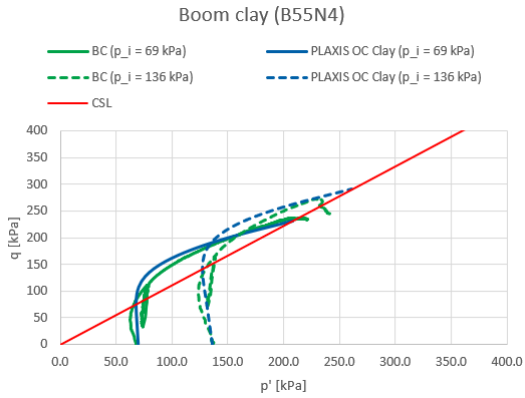

Figure 5.9: Stress path plot

5.1.3. BC Sample B70N6

Intact BC sample (B70N6) were obtained at a depth of 31 - 31.5 m. The initial test conditions used for the analysis are presented in table 5.3. The accompanying output plots are presented in figures 5.10, 5.11 and 5.12

	Test 1	Test 2
p_i' [kPa]	82.3	146.6
POP [kPa]	646	581

Table 5.3: Initial conditions for BC sample B70N6

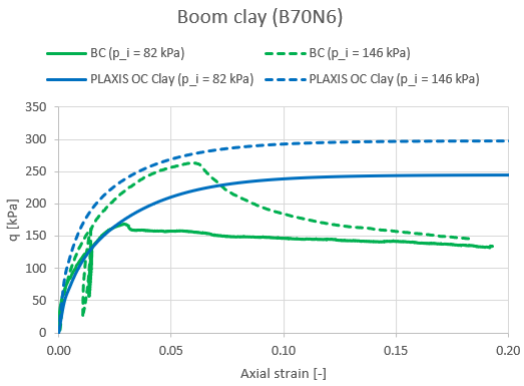

Figure 5.10: Stress-strain plot

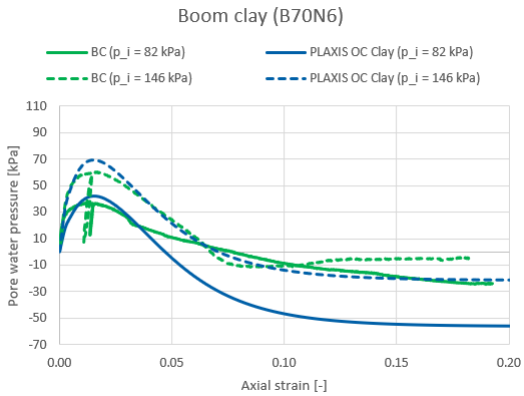

Figure 5.11: Porewater pressure

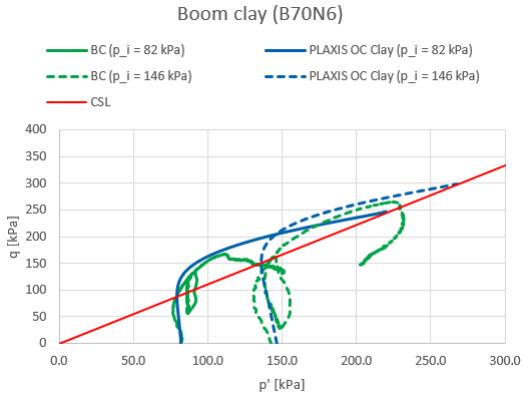

Figure 5.12: Stress path plot

5.1.4. BC Sample B9N6

The BC sample is obtained at a depth of 32.5 and 33 m. The initial test conditions used for the analysis is presented in table 5.4. The corresponding stress-strain, porewater pressure and stress path plots are presented in figures 5.13, 5.14 and 5.15 respectively.

	Test 1	Test 2
p_i' [kPa]	86.3	178.6
POP [kPa]	642	549

Table 5.4: Initial conditions for BC sample B70N6

The validation performed for the BC using test set 1 has shown good agreement with experimental data. B55N4 shows very good agreement with the PLAXIS OC Clay model. The experimental data does not show any premature softening and the stress strain curve is representative of what is observed for the BC. It would not be wrong to say that the test performed on the B55N4 sample is a high quality test.

The B70N6 experimental data shows that the soil sample softens prematurely at about 3% and 6% strain for test 1 and test 2 respectively. This is not an observed behaviour of the BC and causes the model to over predict the strength of the sample.

The B9N6 sample also shows similar trend for test 1 by softening at around 5% strain while test 2 seems to be a bad test as can be seen by the initial stiffness on the the stress strain curve. However, the PLAXIS OC Clay model is still able to simulate the behaviour of the BC and give good excess porewater pressure prediction as seen in the stress - strain, stress path and porewater pressure plots.

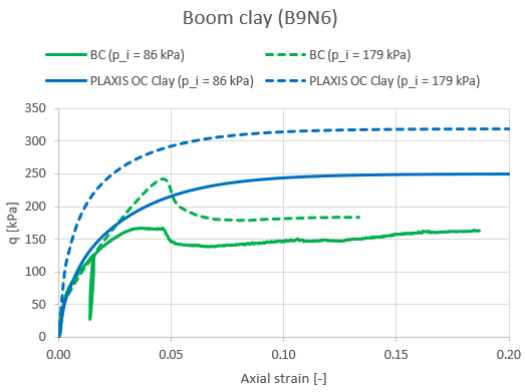

Figure 5.13: Stress-strain plot

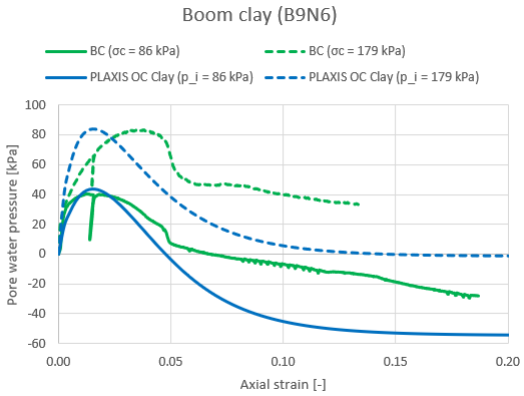

Figure 5.14: Porewater pressure

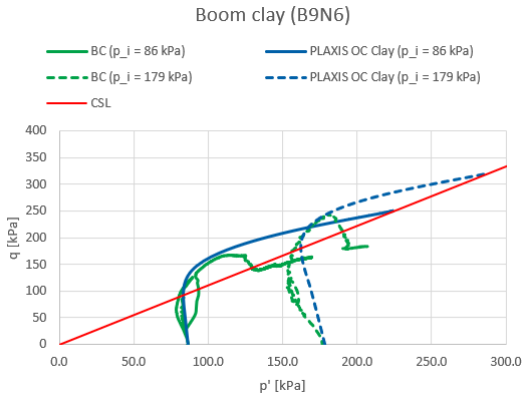

Figure 5.15: Stress path plot

5.2. Test set 2 (Geo_11_063)

The model input parameters obtained from test set 2 samples of the BC which were obtained at a depth range of 21 - 32.5 m is given in table 5.5. The same trend is noticed for all the CU experimental data available for test set 2 BC samples. For brevity, 2 out of the the 7 available CU test simulation will be presented and discussed in this chapter.

Parameter name	Short description	Value	Unit
E_{ur}^{ref}	Unloading/reloading stiffness	31698	kPa
v_{ur}	Poisson's ratio for unloading-reloading	0.2	-
E_{oed}^{ref}	Oedometer stiffness	6338	kPa
φ_{cs}	Effective friction angle at critical state	23	°
$\gamma_{0.7}$	shear strain at $G_s = 0.722G_0$	1.5E-4	-
G_0^{ref}	Reference shear modulus at small strains	120	MPa
p^{ref}	Reference mean effective stress	300	kPa
K_0^{nc}	coefficient of horizontal earth pressure	1	-

Table 5.5: List of PLAXIS OC Clay model input parameters for test set 2

5.2.1. BC Sample B25N4

B25N4 sample is obtained at a depth of 25 -25.5 m. The test conditions used for the CU test simulations are given in table 5.6. The result of the simulation is presented in figures 5.16, 5.17 and 5.18.

There seems to be some disagreement in the stress path presented in figure 5.18 between the numerical and experimental data. The stress path of the BC shows some inclination like a drained test. This may be due to anistropic behaviour observed in weathered undisturbed OC clay samples.

	Test 1	Test 2
p_i' [kPa]	189.2	382.8
POP [kPa]	916	722

Table 5.6: Initial conditions for BC sample B25N4

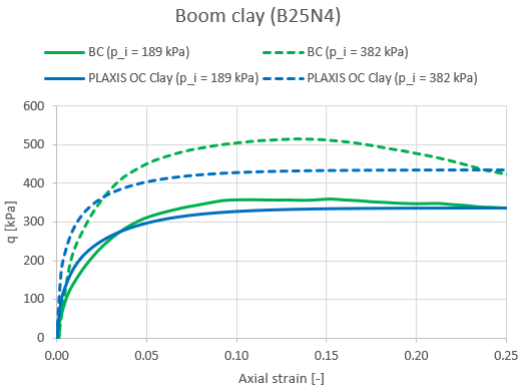

Figure 5.16: Stress-strain plot

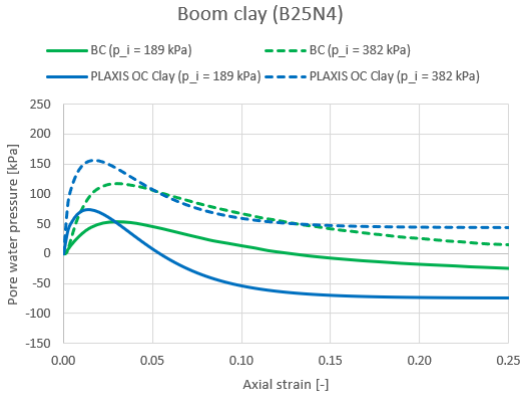

Figure 5.17: Porewater pressure

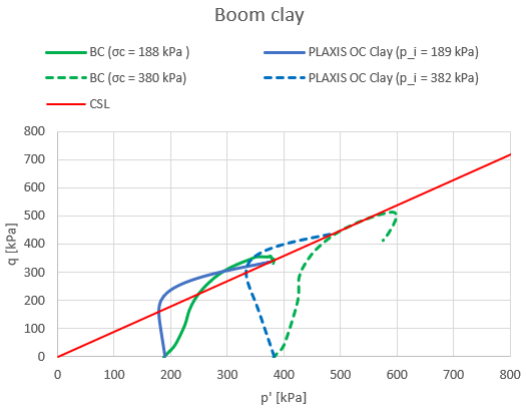

Figure 5.18: Stress path plot

5.2.2. BC Sample B20N6

This BC sample is obtained at the depth of 29.5 - 30 m. The test conditions and the corresponding output plots is given table 5.7 and figures 5.19, 5.20 and 5.21 respectively.

	Test 1	Test 2
p_i' [kPa]	199	410
POP [kPa]	906	695

Table 5.7: Initial conditions for BC sample B20N6

An inspection of the stress - strain plot for the CU test simulations performed for test set 2 samples shows that the model predictions matches up until about 2% strain range before showing some deviation. It is noticed from the porewater pressure plot that the increase of excess porewater pressure during shearing is not as expected. The stress path obtained from both tests shows a slight inclination to the right which is an anisotropic behaviour observed in weathered soils.

The possible reason for this is because the test set 2 (Geo_11_063) BC samples may have been obtained from the top layer of the BC which may be weathered due to the loading (deposition) and unloading (erosion) stress history for the BC. Weathering introduces anisotropy in soil behaviour which

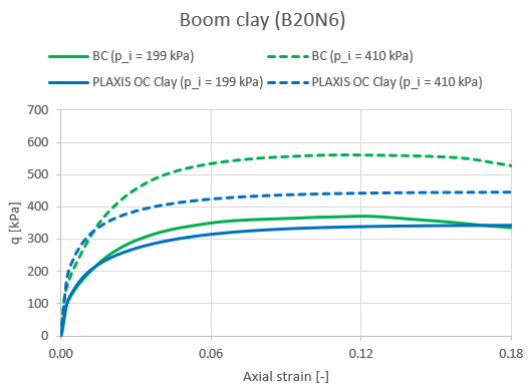

Figure 5.19: Stress-strain plot

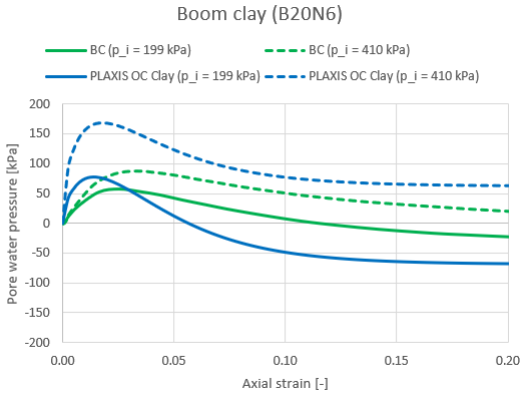

Figure 5.20: Porewater pressure

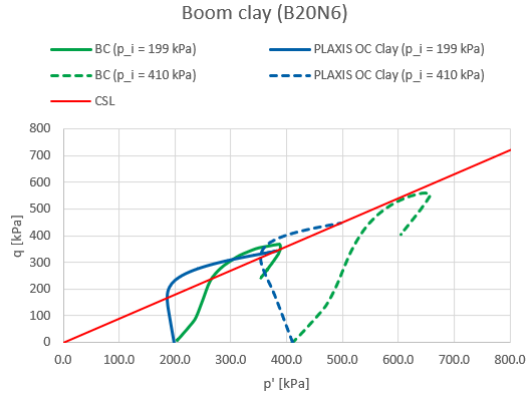

Figure 5.21: Stress path plot

may be what is observed in the stress path of the test set 2 (Geo_11_063) BC samples.

The CPT test data corresponding to the location where the BC samples were obtained was consulted to determine the position of the top layer of the BC with respect to their depth of retrieval. This will help determine whether the samples from test set 2 were obtained closer to the top layer of the BC which may be weathered and thus explain the observation noticed in the CU tests. It is important to mention that test set 2 samples contains pyrites which is are crystals formed due to chemical weathering of clay formations thus confirming that the samples are indeed weathered.

The top of the BC at the location where test set 1 was retrieved is placed at 21.5 m while for test set 2, the top of the BC is at 24 m. This implies that test set 1 BC samples are located deeper in the BC with no fissures while the test set 2 BC samples are located closer to the top layer of the BC which is possibly weathered and thus explains the reason why the stress path in the CU tests displays anisotropic behaviour.

6

Validation of 2D Model of the Trial Excavation

The 2D modelling of the Oosterweel trial excavation alongside the validation of the PLAXIS OC Clay model for the BC is presented in this chapter. Prior to the excavation, piezometers, BAT sensors and extensometers were installed deep into the BC to monitor the changes in porewater pressure and heave respectively which will be experienced during the excavation process. Validation is done by comparing the data from the extensometer and piezometers with the data provided by the 2D model.

6.1. Overview of the Trial Excavation

Figure 6.1 shows the top view of the trial excavation. Notice the octagonal shape and the position of the sensors in the center of the building pit. E1, E2 and E3 are extensometers that measures the vertical displacement experienced as heave, p1 is the piezometer and B1 represents the BAT sensors which both measure the changes in porewater pressures. Inclinometers (i_1, i_2, i_3, i_4, i_5 and i_6) are installed on the sheet pile wall to monitor the horizontal deformation during the excavation.

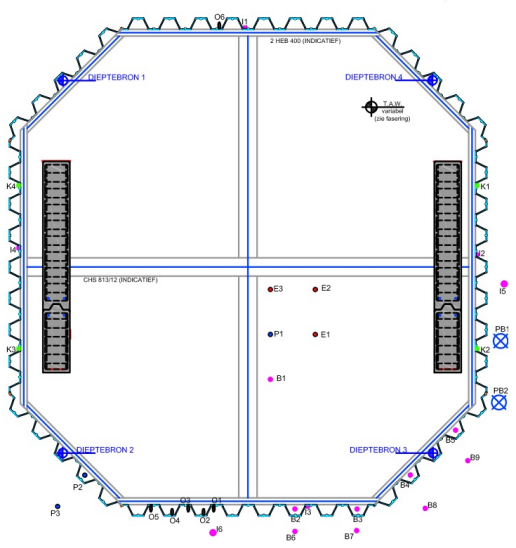

Figure 6.1: Top view of trial excavation

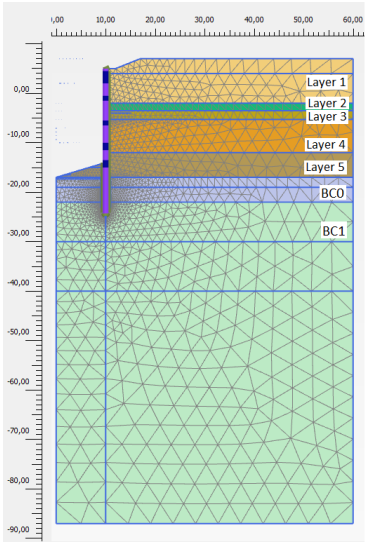

Figure 6.2: 2D axisymmetric model of the trial excavation

A 2D axial symmetric model of the trial excavation is presented in figure 6.2. The top layer is mostly sandy with thin layers of clay. These were modelled using the HSs model while the BC starting at TAW -17m is modelled with the PLAXIS OC clay model.To model the effect of the weathered top layer (BC0) of the BC, the model parameter for test set 2 presented in the previous chapter is used while the deeper

layers (BC1) of the BC are modelled with model parameters obtained from test set 1.

The duration of the excavation process spans over a year and includes about 4 main construction phases which results in 40 calculation stages in the PLAXIS 2D model. The 4 main construction phases are the installation of sheet piles, drainage, installation of struts, and the excavation in steps.

To fully capture time dependent undriained behaviour of the BC, the excavation steps were modeled using consolidation analysis, the water draw-downs (drainage) are modeled with fully coupled flow deformation analysis. It is noteworthy to mention that the soil relative permeability of the different layers present in the 2D model is important for a successful execution of a time dependent analysis in PLAXIS. The permeability of the soils used for the analysis are presented in table 6.1

Layer	Short description	Value	Unit
Layer 1	Sand	1E-2	m/day
Layer 2	Low permeable sand with some clay	1E-5	m/day
Layer 3	Sand	1E-3	m/day
Layer 4	Sand	1E-3	m/day
Layer 5	Sand	1E-3	m/day
BC0	Weathered BC	1.73E-3	m/day
BC1	Intact BC	1.73E-5	m/day

Table 6.1: Permeability of the different soil layers used for the analysis

6.2. Result of Analysis

The results of the analysis at the end of the last phase are presented in this section. Noting that pressure is indicated as negative while suction (or tension) as positive, figure 6.3 shows the active pore pressures at the end of the excavation stage. Very low active water pressure is noticed at the layers of the BC. Figure 6.4 shows the excess porewater pressure and as expected, there is a high excess porewater pressure in the BC inside the excavation around the tip of the sheet pile wall.

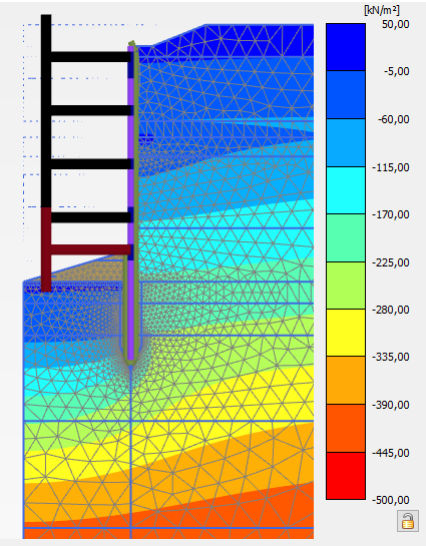

Figure 6.3: Active porewater pressure

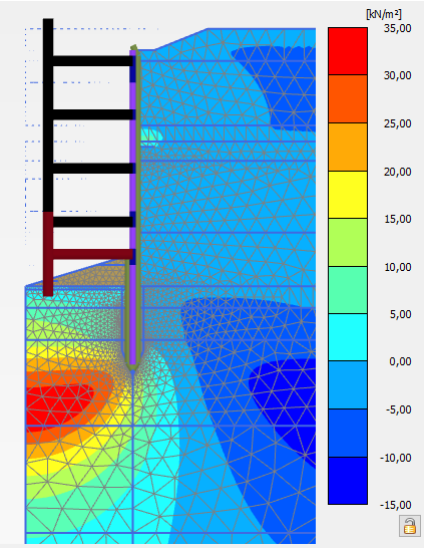

Figure 6.4: Excess porewater pressure

Figures 6.5 and 6.6 shows the mobilized shear strength and total shear strain.
The vertical displacement at the end of the excavation is presented in figure 6.7. As expected, maximum heave is observed at the center of the excavation.

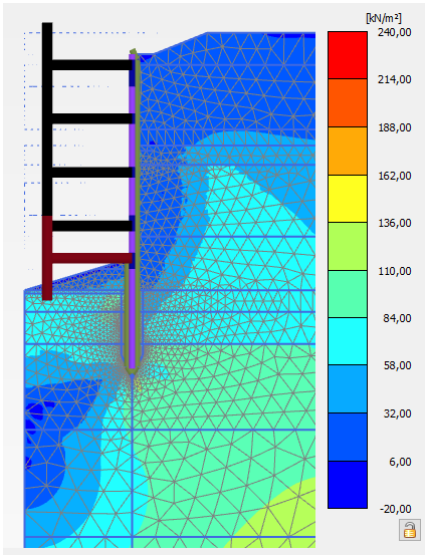

Figure 6.5: Mobilsed shear strength

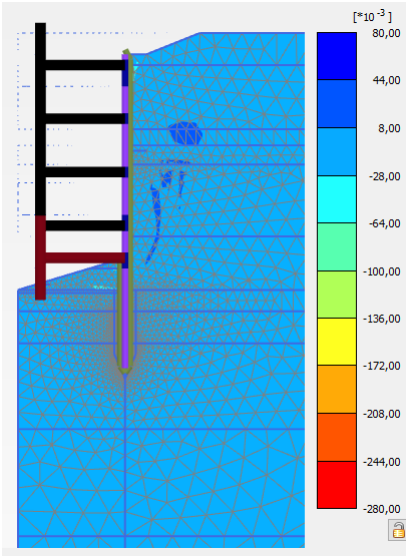

Figure 6.6: Total shear strain

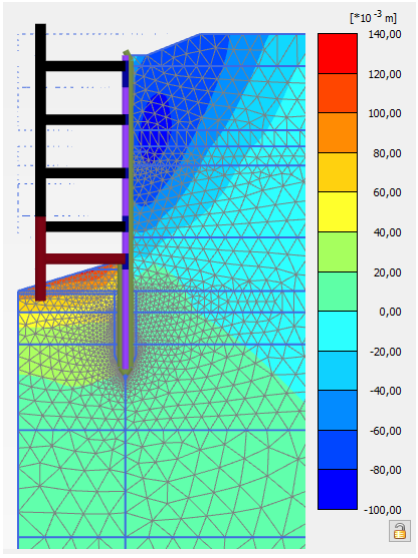

Figure 6.7: Vertical displacement at the end of the excavation

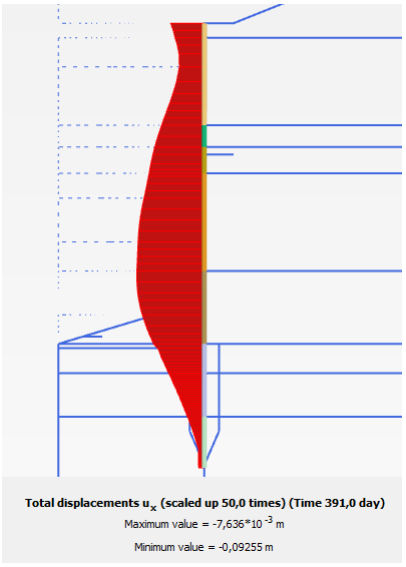

Figure 6.8: Sheet pile wall deflection

6.3. Comparison with Numerical Model

This section compares the analysis obtained from the numerical model with the monitoring data obtained from the Oosterweel trial excavation. In order to make this comparison, it is important to perform a consolidation analysis to account for the time dependent behaviour of OC clays. The porewater pressure and vertical displacement obtained from monitoring data will be compared with the result obtained from the numerical model in the preceding sub sections.

6.3.1. Porewater Pressure

Piezometer P1 installed prior to the commencement of the excavation is used to monitor the porewater pressure changes during the excavation period which lasted more than 365 days. The porewater pressure obtained from the piezometer and BAT sensor at a depth of -18.5 m is compared with the numerical model and presented in figure 6.9. The general trend of the change in the active porewater pressure due to the excavation and dewatering effects in the BC is well captured. However, it seems that the numerical model shows more agreement with the BAT sensor.

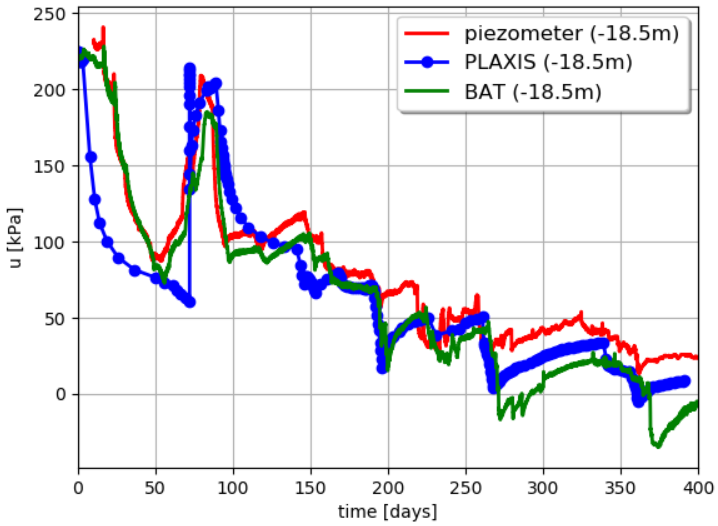

Figure 6.9: changes in porewater pressure during excavation stages

To observe the depth trend in changes of the porewater pressures in the BC, the measurements obtained from the piezometer sensor at various depths in the BC layer are compared with the numerical model in figure 6.10. It can be observed from the in the first 75 days, which simulates dewatering to -12m, excavation and subsequently infill, the numerical model under-predicts the active porewater pressures and is more prominent in the deeper layers.

A reason for this may be attributed to the fact that the piezometer sensors is not able to react quickly to changes in pore pressure due to the low permeability of the BC. However as the construction progresses from 75 days to around 360 days, the porewater pressures obtained from the piezometer and the numerical model seems converge. This seems to further confirms the fact that the piezometers maybe slow to react to the pore pressure changes in the BC layer.

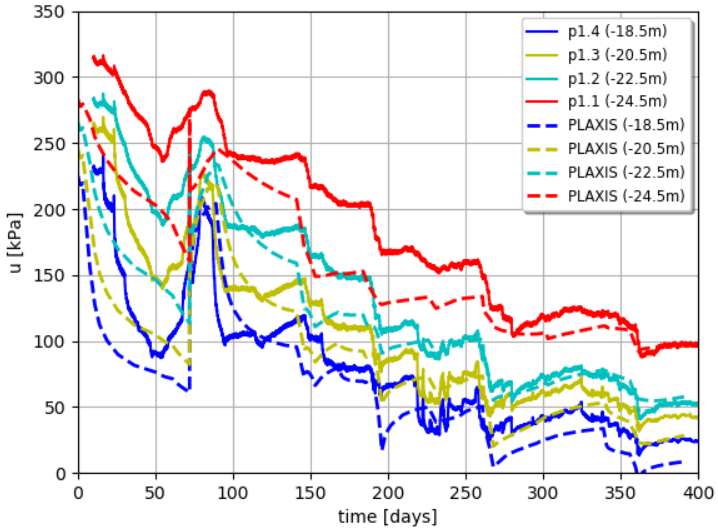

Figure 6.10: changes in porewater pressure during excavation stages at various depths

6.3.2. Soil Displacement

Extensometer E2 is installed to monitor the heave of the BC during the whole excavation process. However, around day 200 (excavation to -12m), it was noticed that the extensometer stopped recording data which prompted the installation of extensometer E4. The data from extensometer E4 and E2 are combined and presented in Figure 6.11 alongside the data obtained from the numerical model.

It is important to mention that the incremental measurements recorded by the extensometer during the various excavation and dewatering stages are not very precise but the heave recorded at the end of the excavation process is consistent. Figure 6.11 shows that the numerical model is able to predict the heave in the BC over time and as can be seen, the final heave predicted by the numerical model at the end of the excavation stages shows agreement with field data with a value of 62 mm.

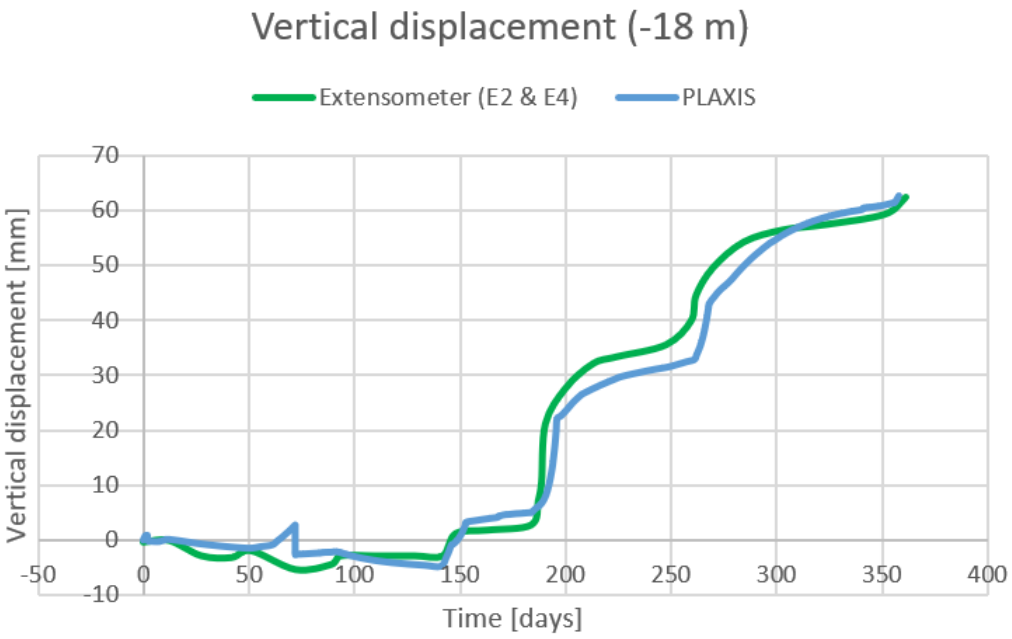

Figure 6.11: Comparison of the heave measured by the extensometer (E2 & E4) with numerical model

6.3.3. Deflection of Sheet Pile Wall

The deflection of the sheet pile wall obtained from the numerical model is compared with the measured data and presented in figure 6.12. Modeling the excavation as a 2D axis-symmetric model has consequences on the deflection of the sheet pile wall obtained from the numerical model which can be attributed to the hoop forces. In an attempt to compensate for this, point displacements were prescribed at some of the stages during the calculation in the numerical model.

Although the trend in the horizontal deflection of the sheet pile wall obtained from the numerical model and the measured data are comparable, it seems that the prescribed displacements does not fully compensate for the hoop forces and as such, the numerical model under estimates the maximum deflection of the sheet pile wall. To obtain a more realistic sheet pile wall deflection, it is advised to use a 3D numerical model as this will fully account for the hoop forces and give a better estimation of the wall deflection.

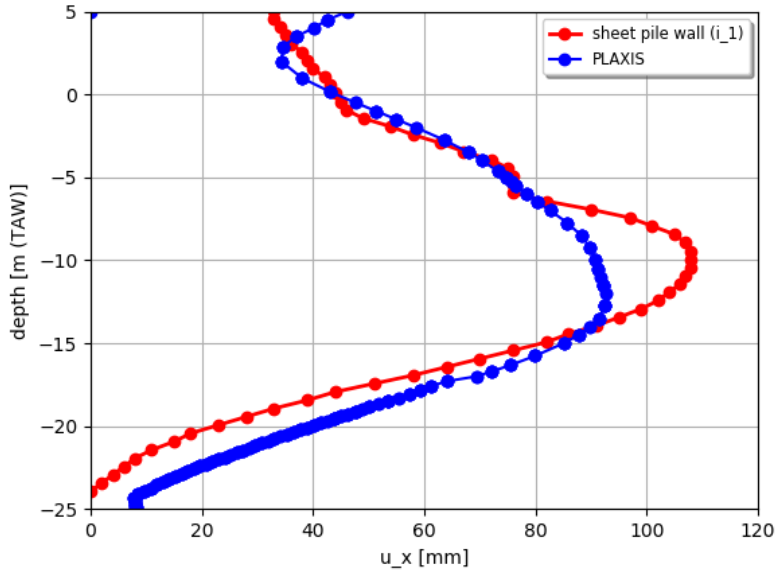

Figure 6.12: Deflection of sheet pile wall

This chapter has demonstrated the ability of the PLAXIS OC Clay model to reproduce the behaviour of the OC BC in 2D boundary value problem of the Oosterweel trial excavation. The porewater pressure changes during the excavation stages as well as the vertical displacement measured at the top of the BC at the end of the excavation process are well captured and thus concludes the validation of the PLAXIS OC Clay model for the BC.

7

Conclusion

This research aimed at obtaining a soil model capable of reproducing the undrained behaviour of OC cohesive soil has led to the formulation and validation of the PLAXIS OC Clay model for the BC. The model has demonstrated to be capable of simulating the drained and undrained behaviour of OC clays and is also not sensitive to input parameters when compared to the HASP model as seen in the sensitivity analysis.

The PLAXIS OC Clay model input parameters which can easily be derived from CU and oedometer tests including the method of parameter determination has been well substantiated. The simulation of CU tests for BC has shown good agreement with experimental data. An evaluation of the stress strain curve at small strain shows that a better agreement is observed for the PLAXIS OC Clay model in comparison to the HASP model which can be attributed to the small strain formulation addition to the model.

It is important to mention that a peculiar behaviour was noticed in the stress path of test set 2 BC samples which were obtained from the top layer of the BC. The inclination of the stress path can be attributed to anisotropy which are characteristics usually observed in weathared OC clays. Test set 2 BC samples were found to contain pyrites which are clay minerals formed due to chemical weathering and thus confirms the fact that the samples are indeed weathered and hence the anisotropic behaviour observed in the stress path plot.

Further validation of the model was done by modelling the BC in the Oosterweel trial excavation. The porewater pressures changes and the vertical displacement or heave of the top layer of the BC caused by the excavation effects were measured and compared with the numerical model. The total heave measured at the end of the excavation is in accordance with the heave obtained from the numerical model. Furthermore, the trend in the changes of pore water pressures in the boom clay during the excavation process is also well captured.

On a final note, the unloading - reloading behaviour of the PLAXIS OC Clay model is not very realistic and is recommended for further research and improvement. This behaviour may be due to the consequence of the elastoplastic formulation of the model which implies that elastic and plastic strains develop from the onset of loading. Considering that unloading - reloading can be said to be elastic, a distinction between elastic and plastic loading in the model may improve its behaviour in this context.

Bibliography

[1] T. Benz. *Small-Strain Stiffness of Soils and its Numerical Consequencies*. PhD thesis, Universitat Stuttgart, 2007.

[2] A.S Greeuw. Geomechanical unloading behaviour of boom clay for excavations. Technical report, Technical University, Delft, Netherlands, 2015.

[3] G. Gudehus. A comprehensive constitutive equation for granular materials. *Soils And Foundations*, 36(1):1 – 12, 1996.

[4] G. Gudehus and D. Mason. Graphical representation of constitutive equations. *Geotechnique*, 59 (2):147 – 151, 2009.

[5] Mike Jefferies and Ken Been. *Soil liquefaction, a critical state approach*. CRC Press, 2 edition, 2015. ISBN 9781482213676.

[6] S. Jockovic and M. Vukicevic. Bounding surface model for overconsolidated clays with new state parameter formulation of hardening rule. *Computers and Geotechnics*, 83:16 – 29, 2017.

[7] X.S Li and Y.F Dafalias. Dilatancy for cohesionless soils. *Geotechnique*, 50:449 – 460, 2000.

[8] D. Masin. Clay hypoplasticity with explicitly defined asymptotic states. *Acta Geotechnica manuscript*, 62:549 – 553, 2012.

[9] R. De Nijs, F. Kaalberg, G. Osselaer, J. Couck, and K. van Royen. Geotechical monitoring of a trial pit excavation toward the boom clay in antwerp (belgium). Technical report, THV throts, Witteveen + Bos, BAM NV, Flemish Government, 2015.

[10] R. Nova and D.M Wood. A constitutive model for sand in triaxial compression. *International Journal Numerical and Analytical Methods Geomech*, 3:255 – 278, 1979.

[11] R. H. G. Parry. Correspondence. *Geotechnique*, 8:183 – 186, 1958.

[12] Jockovic Sanja and Vukicevic Mirjana. Critical state constitutive model for overconsolidated clays-hasp model. *XVI Danube - European Conference on Geotechnical Engineering*, 2018.

[13] A. Truty and R. Obrzud. Improved formulation of the hardening soil model in the context of modelling the undrained behaviour of cohesive soils. *Studia Geotechnica et Mechanica*, 37:449 – 460, 2015.

[14] G. Vilhar and R. Brinkgreve. Constitutive model for overconsolidated clays, beta version 2.1. Technical report, PLAXIS bv, a Bentley Systems company, Delft, Netherlands, 2019.

[15] D. Muir Wood. *Soil Behaviour and Critical State Soil Mechanics*. Cambridge University Press, 1 edition, 1990. ISBN 0-521-33782-8.

Appendices

.1. HASP model implementation in python script

The computational steps for integrating along imposed stress path for undrained condition are given below.

1. Specify initial conditions p'_{init}, q_{init}
2. Specify increment $\Delta p'_{initial}$
3. Compute the effective mean stress $p'_1 = p'_{init} - \Delta p'_{init}$
4. Compute the state parameters $\Psi_{i+1} = v + \lambda ln p'_{i+1} - \Gamma$; $\bar{\Psi}_{i+1} = (\lambda - \kappa) ln(2M^2/(M^2 + \eta_i^2))$
5. Compute OCR $R_{i+1} = exp((\bar{\Psi}_{i+1} - \Psi_{i+1}/(\lambda - \kappa))$
6. Compute hardening coefficient $\omega_{i+1} = (1 + (\bar{\Psi}_{i+1} - \Psi_{i+1})/\bar{\Psi}_{i+1})R_{i+1}$
7. Compute alpha $\alpha_{i+1} = (\lambda - \kappa)/(\omega_{i+1}\kappa + (\lambda - \kappa))$
8. Compute the stress ratio $\eta_{i+1} = \sqrt{\left((p'_i/p'_{i+1})^{1/\alpha}(M^2 + \eta_i^2) - M^2\right)}$
9. Compute deviatoric stress $q_{i+1} = p'_{i+1}\eta_{i+1}$
10. Compute volumetric strains $\varepsilon^p_{v,i+1} = \varepsilon^p_{v,i} + \Delta\varepsilon^p_v$[1] ; $\varepsilon^e_{v,i+1} = -\varepsilon^p_{v,i+1}$
11. Compute increment in mean stress $\Delta p' = \Delta\varepsilon^e_v P'_i \nu/\kappa$
12. Compute shear modulus $G_{i+1} = 3(1 - 2\mu)v_{i+1}p'_{i+1}/2(1 + \mu)\kappa$
13. Compute shear strains $\varepsilon^e_{q,i+1} = \varepsilon^e_{q_i} + \Delta q/(3G_{i+1})$; $\varepsilon^p_{q,i+1} = \varepsilon^e_{q_i} + \Delta\varepsilon^p_q$[2]; $\varepsilon_{q,i+1} = \varepsilon^e_{q,i+1} + \varepsilon^p_{q,i+1}$
14. Compute total mean stress $p_{i+1} = p_{init} + q_{i+1}/3$
15. Compute pore pressure $u_{i+1} = p_{i+1} - p'_{i+1}$

[1] computed with equation 3.7
[2] computed with equation 3.8

Appendix 2: Python Script for the HASP model (undrained conditions)

```
import numpy as np
import math
import matplotlib.pyplot as plt

# ----------------------------------------------
# Input material parameters
# ----------------------------------------------

lambda_1 = 0.077   # Slope of virgin Compression line
kappa = 0.022  # Slope of unloading reloading line in
isotropic compression
phi = 26.5
phi_crit = 28  # Critical state friction angle
M = 6 * np.sin(phi_crit*np.pi/180)/(3 -
np.sin(phi_crit*np.pi/180))      # Slope of Critical state
line
Gamma = 2.043  # Reference specific volume for p' = 1 kPa on
critical state line
v = 0.2        # Poisson's ratio

# ----------------------------------------------
# Initial Conditions
# ----------------------------------------------
p_init = 69.4  # kPa
e_0 = 0.6
q_init = 0    # kPa
delta_p_init = 0.002
p_ref = 300  # kPa
v_ref = 1 + e_0
v_k = v_ref + kappa*np.log(p_ref)
v_0 = v_k - kappa*np.log(p_init)

# ------------------------------------------------------------
# initialization
# ------------------------------------------------------------
n = 1000

p_0 = p_init
p_1 = p_init - delta_p_init
p = [p_0, p_1]
eta_0 = 0.00

psi_0 = (v_0 + lambda_1 * np.log(p_0)) - Gamma
psi_01 = (v_0 + lambda_1 * np.log(p_0)) - Gamma
psi_1 = (v_0 + lambda_1 * np.log(p_1) - Gamma)
psi = [psi_0, psi_1]
psi_conjug_0 = (lambda_1 - kappa) * np.log((2 * M**2)/(M**2 +
eta_0 ** 2))
```

```
psi_conjug_1 = (lambda_1 - kappa) * np.log((2 * M**2)/(M**2 +
eta_0 ** 2))

psi_conjug = [psi_conjug_0, psi_conjug_1]

OCR_i_0 = (2 * math.exp(psi_0/(kappa - lambda_1)))
OCR_i_1 = (2 * math.exp(psi_1/(kappa - lambda_1)))
OCR_i = [OCR_i_0, OCR_i_1]
OCR_conjug_0 = (2 * math.exp(psi_conjug_0/(kappa - lambda_1)))
OCR_conjug_1 = (2 * math.exp(psi_conjug_1/(kappa - lambda_1)))
OCR_conjug = [OCR_conjug_0, OCR_conjug_1]
OCR_0 = OCR_i_0/OCR_conjug_0
OCR_1 = OCR_i_1/OCR_conjug_1
OCR = [OCR_0, OCR_1]

omega_0 = ((1 + (psi_conjug_0 - psi_0)/psi_conjug_0)*OCR_0)
omega_1 = ((1 + (psi_conjug_1 - psi_1)/psi_conjug_1)*OCR_1)
omega = [omega_0, omega_1]

alpha_0 = 0
alpha_1 = ((lambda_1 - kappa)/((omega_1*kappa)+(lambda_1 -
kappa)))
alpha = [alpha_0, alpha_1]

eta_0_square = ((p_0/p_0)**0 * (M**2 + eta_0) - M**2)
eta_0 = np.sqrt(eta_0_square)

eta_1_square = (((p_0/p_1)**(1/alpha_1)) * (M**2 + eta_0**2) -
M**2)
eta_1 = (np.sqrt(eta_1_square))
eta_square = [eta_0_square, eta_1_square]
eta = [eta_0, eta_1]


q_0 = eta_0 * p_0
q_1 = (eta_1 * p_1)
q = [q_0, q_1]

eps_v_p_0 = 0
eps_v_p_1 = (eps_v_p_0 + ((lambda_1 - kappa)/(v_0 * p_1 *
omega_1) * (1/(M**2 + eta_1**2))*((M**2 - eta_1**2)*(p_1 -
p_0) + 2 * eta_1 * (q_1 - q_0))))
eps_v_p = [eps_v_p_0, eps_v_p_1]

eps_v_e_init = 0
eps_v_e_0 = - eps_v_p_0
eps_v_e_1 = -eps_v_p_1
eps_v_e = [eps_v_e_0, eps_v_e_1]

if psi_0 < 0:
    dp_0 = (eps_v_e_0 - eps_v_e_init) * v_0 / kappa * p_init
```

```
else:
    dp_0 = 0

if psi_1 < 0:
    dp_1 = ((eps_v_e_1 - eps_v_e_0) * v_0 / kappa * p_1)
else:
    dp_1 = 0

dp = [dp_0, dp_1]

eps_v_0 = eps_v_e_0 + eps_v_p_0
eps_v_1 = eps_v_e_1 + eps_v_p_1
eps_v = [eps_v_0, eps_v_1]

G_init = 3 * (1 - 2 * v)/(2*(1+v)) * v_0 * p_init/kappa
G_0 = 3 * (1 - 2 * v)/(2*(1+v)) * v_0 * p_0/kappa
G_1 = 3 * (1 - 2 * v)/(2*(1+v)) * v_0 * p_1/kappa
G = [G_0, G_1]

eps_q_e_0 = 0
eps_q_e_1 = eps_q_e_0 + (np.abs(q_1 - q_0)) / (3 * G_1)
eps_q_e = [eps_q_e_0, eps_q_e_1]

eps_q_p_0 = 0
eps_q_p = [eps_q_p_0]

eps_q = (eps_q_e_0 + eps_q_p_0)

ptot_0 = p_init + q_0/3
ptot = [ptot_0]


# ---------------------------------------------------------------
# Loop containing the governing parameter and the computed quantities
# ---------------------------------------------------------------
for i in range(2, n):
    p1 = p[i-1] + dp[i-1]
    p.append(p1)

    psi1 = v_0 + lambda_1 * np.log(p[i]) - Gamma
    psi.append(psi1)

    psi_conjug1 = (lambda_1 - kappa) * np.log(2*M**2/(M**2 +
eta[i-1]**2))
    psi_conjug.append(psi_conjug1)

    OCR_i1 = 2 * math.exp(psi[i]/(kappa - lambda_1))
    OCR_i.append(OCR_i1)

    OCR_conjug1 = 2 * math.exp(psi_conjug[i-1]/(kappa -
lambda_1))
```

```
    OCR_conjug.append(OCR_conjug1)

    OCR1 = OCR_i[i]/OCR_conjug[i]
    OCR.append(OCR1)

    omega1 = (1 + (psi_conjug[i] - psi[i])/psi_conjug[i]) *
OCR[i]
    omega.append(omega1)

    alpha1 = (lambda_1 - kappa)/((omega[i]*kappa)+(lambda_1 -
kappa))
    alpha.append(alpha1)

    eta_square1 = ((p[i-1]/p[i])**(1/alpha[i-1]) * (M**2 +
eta[i-1]**2) - M**2)
    eta_square.append(eta_square1)

    eta1 = np.sqrt(eta_square[i])
    eta.append(eta1)

    q1 = eta[i] * p[i]
    q.append(q1)

    eps_v_p1 = eps_v_p[i-1] + ((lambda_1 - kappa) / (v_0 *
p[i] * omega[i]) * (1 / (M ** 2 + eta[i] ** 2)) * (
                (M ** 2 - eta[i] ** 2) * (p[i] - p[i-1]) + 2 *
eta[i] * (q[i] - q[i-1])))
    eps_v_p.append(eps_v_p1)

    eps_v_e1 = - eps_v_p[i]
    eps_v_e.append(eps_v_e1)

    if psi[i] < 0:
        dp1 = (eps_v_e[i] - eps_v_e[i-1]) * v_0/kappa * p[i-1]
    else:
        dp1 = 0
    dp.append(dp1)

    eps_v1 = eps_v_p[i] + eps_v_e[i]
    eps_v.append(eps_v1)

    G1 = 3*(1-2*v)/(2*(1+v))*v_0*p[i]/kappa
    G.append(G1)

    eps_q_e1 = eps_q_e[i-1] + (np.abs(q[i]-q[i-1])/(3*G[i]))
    eps_q_e.append(eps_q_e1)

# ----------------------------------------------------------
# Computation of axial strain
# ----------------------------------------------------------
```

```
for j in range(1, n-1):
    eps_q_p1 = eps_q_p[j-1] + ((lambda_1 - kappa)/(v_0 * p[j]
* omega[j+1])) * (1/(M**2 + eta[j]**2)) * ((2*eta[j] * (p[j] -
p[j-1])) + (4 * eta[j]**2)/(M**2 - eta[j]**2)*(q[j] - q[j-1]))
    eps_q_p.append(eps_q_p1)

eps_q_p_fin = eps_q_p[-1] + ((lambda_1 - kappa)/(v_0 * p[-1] *
omega[-1])) * (1/(M**2 + eta[-1]**2)) * ((2*eta[-1] * (p[-1] -
p[-2])) + (4 * eta[-1]**2)/(M**2 - eta[-1]**2)*(q[-1] - q[-
2]))
eps_q_p.append(eps_q_p_fin)

eps_q1 = [x + y for x, y in zip(eps_q_e[1:], eps_q_p[1:])]
eps_q1.insert(0, eps_q)

for k in range(0, n):
    ptot_1 = p_init + q[k] / 3
    ptot.append(ptot_1)
u = [x - y for x, y in zip(ptot, p)]


# ---------------------------------------------------------------
# Critical state line
# ---------------------------------------------------------------
p_crit = np.linspace(0, 900, 6)
q_crit = M * np.array(p_crit)


# ---------------------------------------------------------
# Plots
# ---------------------------------------------------------
#  stress strain plot
fig, (ax1) = plt.subplots()
ax1.plot(eps_q1, q, 'b', linewidth=1.5, label='HASP (python
script)')
ax1.grid()
plt.xlabel("axial strain [-]")
plt.ylabel("q [kPa]")
ax1.legend(loc='upper right', shadow=True, fontsize='large')
ax1.set_xlim(0, 0.25)
ax1.set_ylim(0, 350)
plt.savefig('stress_strain1')
plt.show()

#  stress path plot
fig2, (ax2) = plt.subplots()
ax2.plot(p, q, 'b', linewidth=1.5, label='HASP (python
script)')
ax2.plot(p_crit, q_crit, 'r', linewidth=1.5, label='CSL')
plt.xlabel("p' [kPa]")
plt.ylabel("q [kPa]")
```

```
ax2.set_xlim(0, 350)
ax2.set_ylim(0, 300)
ax2.grid()
ax2.legend(loc='upper left', shadow=True, fontsize='large')
plt.savefig('stress_path1')
plt.show()

# Porewater pressure plot
fig3, (ax3) = plt.subplots()
ax3.plot(eps_q1, u, 'b', linewidth=1.5, label='HASP (python
script)')
ax3.legend(loc='upper right', shadow=True, fontsize='large')
ax3.grid()
plt.xlabel("axial strain [-]")
plt.ylabel("P_w [kPa]")
ax3.set_xlim(0, 0.25)
ax3.set_ylim(-100, 80)
plt.savefig('P_w')
plt.show()

# ------------------------------------------------------------
```